UNIVERSIDADE ESTADUAL DE CAMPINAS

Faculdade de Engenharia Química

Flávia Nogueira Braga

Study of diffusion aspects in confined media subject to external electric potential for application in catalysis via Molecular Dynamics simulations

Estudo dos aspectos difusionais em meios confinados sujeitos a potenciais elétricos externos para aplicação em catálise via simulações de Dinâmica Molecular

CAMPINAS

2022

Flávia Nogueira Braga

Study of diffusion aspects in confined media subject to external electric potential for application in catalysis via Molecular Dynamics simulations

Estudo dos aspectos difusionais em meios confinados sujeitos a potenciais elétricos externos para aplicação em catálise via simulações de Dinâmica Molecular

Dissertation presented to the Faculty of Chemical engineering of the University of Campinas in partial fulfillment of the requirements for the degree of Master in Chemical engineering

Dissertação apresentada à Faculdade de Engenharia Química da Universidade Estadual de Campinas como parte dos requisitos exigidos para a obtenção do título de Mestra em Engenharia Química

Supervisor: Prof. Dr. Luís Fernando Mercier Franco
Co-supervisor: Prof. Dr. Gustavo Doubek

ESTE TRABALHO CORRESPONDE À VERSÃO FINAL DA DISSERTAÇÃO DEFENDIDA PELA ALUNA FLAVIA NOGUEIRA BRAGA, E ORIENTADA PELO PROF. DR. LUÍS FERNANDO MERCIER FRANCO

Campinas

2022

Ficha catalográfica
Universidade Estadual de Campinas
Biblioteca da Área de Engenharia e Arquitetura
Rose Meire da Silva - CRB 8/5974

Braga, Flávia Nogueira, 1995-
B73s Study of diffusion aspects in confined media subject to external electric potential for application in catalysis via molecular dynamics simulations / Flávia Nogueira Braga. – Campinas, SP : [s.n.], 2022.

Orientador: Luís Fernando Mercier Franco.
Coorientador: Gustavo Doubek.
Dissertação (mestrado) – Universidade Estadual de Campinas, Faculdade de Engenharia Química.

1. Dinâmica molecular. I. Franco, Luís Fernando Mercier, 1988-. II. Doubek, Gustavo, 1984-. III. Universidade Estadual de Campinas. Faculdade de Engenharia Química. IV. Título.

Informações para Biblioteca Digital

Título em outro idioma: Estudo dos aspectos difusionais em meios confinados sujeitos a potenciais elétricos externos para aplicação em catálise via simulações de dinâmica molecular
Palavras-chave em inglês:
Molecular dynamics
Área de concentração: Engenharia Química
Titulação: Mestra em Engenharia Química
Banca examinadora:
Luís Fernando Mercier Franco [Orientador]
André Rodrigues Muniz
Mariana Conceição da Costa
Data de defesa: 11-08-2022
Programa de Pós-Graduação: Engenharia Química

Identificação e informações acadêmicas do(a) aluno(a)
- ORCID do autor: https://orcid.org/0000-0001-5381-7178
- Currículo Lattes do autor: http://lattes.cnpq.br/8776408893834375

Flávia Nogueira Braga

Study of diffusion aspects in confined media subject to external electric potential for application in catalysis via Molecular Dynamics simulations

Data de aprovação: 11 / 08 / 2022

BANCA EXAMINADORA

Prof. Dr. Luís Fernando Mercier Franco
Presidente (Unicamp)

Prof. Dr. André Rodrigues Muniz
Membro (UFRGS)

Prof. Dra. Mariana Conceição da Costa
Membro (Unicamp)

CAMPINAS

2022

A Ata da Defesa, assinada pelos membros da Comissão Examinadora, consta no SIGA/Sistema de Fluxo de Dissertação/Tese e na Secretaria do Programa da Unidade.

Dedico este trabalho à minha família, que sempre me apoiou incondicionalmente, e ao meu marido, que foi meu ponto de apoio durante todo meu mestrado.

Acknowledgements

(in Portuguese)

A Deus por ter sempre me abençoado e guiado todo o meu caminho.

À minha família, principalmente meus pais, Paulo e Maria José, por terem sempre apoiado meus sonhos, se desdobrado para me dar as condições para que eles se realizassem, nunca deixando que eu desistisse deles.

Ao meu marido, João, por ter acreditado mais em mim do que eu mesma, por sempre ser meu ponto de paz e meu porto seguro. Minha eterna graditão por ter estado ao meu lado e me compreendido tanto durante todo esse caminho.

Aos meus amigos, que trago sempre comigo e que são ótimos ouvintes, conselheiros e grandes entusiastas apoiadores dos meus sonhos.

Aos integrates do Laboratório de Engenharia de Sistemas Complexos (LESC) por todas as discussões, ideias e ajuda que com certeza contribuíram para o resultado final desse trabalho. À Marcelle, especialmente, por toda paciência, conhecimento compartilhado e por fornecer os códigos base para o cálculo do coeficiente de difusão. À Larissa pela amizade e por ter sido minha companhia constante em todo o mestrado, mesmo à distância. Ao Felipe Mourão por ter sido um ótimo companheiro de laboratório por tantos meses e pelo auxílio no desenvolvimento dos códigos de análise dos dados. Ao Luiz Guilherme, por sempre estar disposto a ajudar e por ter sido um grande apoio no aprendizado da utilização dos softwares.

Ao meu orientador, Professor Luís Fernando, por todo o ensinamento transmitido e por toda a paciência e compreensão, sendo mais do que um orientador nesses dois anos. Sempre será uma grande inspiração para mim como pessoa e como profissional.

Ao meu coorientador, Professor Gustavo, por todo o conhecimento compartilhado e por ter agregado em meu trabalho em diversos aspectos.

Aos membros da minha banca de qualificação, Professor André Muniz e Munir Skaf, pelos valiosos comentários a respeito do meu projeto. Ao Professor André por ter aceitado retornar como membro na minha defesa. À Professora Mariana Costa por também ter aceitado ser parte da banca de defesa.

Ao apoio financeiro do Programa de Recursos Humanos da Agência Nacional de Petróleo, Gás natural e Biocombustíveis (PRH-ANP), suportado com recursos provenientes do investimento de empresas petrolíferas qualificadas na Cláusula de P, D&I da Resolução ANP no 50/2015 (PRH 29.1 - Consultar EDITAL Nº 1/2018/PRH-ANP; Convênio Finep/Funcamp/FEQ Ref. 5485).

Ao "Centro Nacional de Processamento de Alto Desempenho em São Paulo (Cenapad-SP)" por contribuir com recursos computacionais para obtenção de parte dos resultados desse trabalho. Assim como ao "Laboratório de Computação Científica (LNCC/MCTI, Brasil)" por fornecer recursos computacionais de alta desempenho do supercomputador SDumont.

“O começo de todas as ciências é o espanto de as coisas serem o que são.” – Aristóteles

Eu, Flávia Nogueira Braga, declaro que esse trabalho é de autoria própria e que as partes que não o são foram devidamente referenciadas ao longo do trabalho.

Resumo

O estudo de fluidos confinados tem aplicações em diversas áreas da ciência e da engenharia. A importância de entender o comportamento desses sistemas não se restringe a aspectos fundamentais, mas também pode ser estendida ao projeto de processos industriais inovadores. A catálise sobressai-se como uma importante aplicação de fluidos confinados. Em particular, a catálise eletrostática é uma das áreas menos desenvolvidas da química sintética, mas tem grande potencial para ser uma alternativa para manipular a seletividade de produtos e as taxas de reação de processos com uma maior eficiência energética. O efeito do confinamento permanece, no entanto, difícil de medir ou predizer. Neste sentido, as simulações de Dinâmica Molecular constituem uma valiosa técnica computacional para analisar esses sistemas. Baseada em mecânica estatística, esta ferramenta permite a análise do comportamento de fluidos considerando partículas no nível atomístico. Portanto, nesta dissertação, a Dinâmica Molecular foi empregada para realizar um estudo exploratório do comportamento de fluidos confinados submetidos a um campo elétrico externo. O sistema de interesse para este estudo foi o da síntese de Fischer-Tropsch, como parte do processo gás-líquido para transformar gás natural em hidrocarbonetos de cadeias maiores. Este processo permite obter combustíveis menos poluentes e petroquímicos em geral. Misturas de água com hidrocarbonetos, modelados por metano, *n*-butano e *n*-pentano, confinados em poros de grafeno, foram utilizados para avaliar a influência do campo elétrico externo no comportamento geral de confinamento. Os resultados mostraram que a aplicação do campo, de fato, alterou a separação de fases desses sistemas, causando uma adsorção de água no grafeno, uma superfície naturalmente hidrofóbica. Um novo leque de aplicações surge com estes resultados, por exemplo, para a uso de campos elétricos para a recuperação de catalisadores em refino de petróleo.

Abstract

The study of confined fluids has applications in several areas of science and engineering. The importance of understanding the behavior of these systems is not restricted to fundamental aspects, but can also be extended to the design of innovative industrial processes. Catalysis stands out as an important application of confined fluids. In particular, electrostatic catalysis is one of the less developed areas of synthetic chemistry but has great potential to be an alternative to manipulate products selectivity and reaction rates in processes obtaining higher energy efficiency than those thermally-based. The effect of confinement remains, however, difficult to measure or predict. In this sense, Molecular Dynamics simulations constitute a valuable set of computational techniques to analyse these systems. Based on statistical mechanics, this tool allows the analysis of the behavior of fluids by considering particles at an atomistic level. Therefore, in this dissertation, Molecular Dynamics was employed to conduct an exploratory study of the behavior of confined fluids subjected to an external electric field. The system of interest for this study was the Fischer-Tropsch synthesis, as a part of the gas to liquid process to transform natural gas into larger hydrocarbons. The direct applications of this process are more environmentally friendly fuels and petrochemicals in general. A mixture of water with hydrocarbons, modeled by methane, *n*-butane, and *n*-pentane, confined in a graphene slit pore is chosen to assess the influence of the external electric field in the general confinement behavior. The results showed that the application of the field changed the phase separation of these systems, causing an adsorption of water on graphene, a hydrophobic surface. A new range of application emerges with these results, for example, for the use of electric fields to recovery of catalysts in oil refining.

List of Figures

List of Tables

Contents

1 Introduction

Fluids confined in porous materials play an increasingly important role in several areas of science and engineering [Wang and Fichthorn, 2000]. Their application includes the understanding of phenomena in biology, such as permeability of ion channels and protein stability. In chemistry and chemical engineering, confined fluids may also be found in materials on a nanometric scale for catalysis. In geology, on another hand, they are relevant to the study of porous rocks such as in unconventional oil and gas reservoirs [Foroutan et al., 2017].

Large knowledge gaps, however, remain regarding the behavior of these systems [Qiao et al., 2019]. Therefore, the interest and the effort in the study of confined fluids has grown and gained momentum in the recent decades [Wang and Fichthorn, 2000]. Since experimental measurements are difficult to be executed, and the behavior is difficult to predict, confinement effects have been largely studied by atomistic theories and simulation methods.

Molecular Dynamics simulations, for instance, have been used to investigate diffusive behavior under both equilibrium and non-equilibrium conditions in confined fluids, in addition to simultaneous diffusion and reaction, capillary condensation, and nucleation [Gubbins et al., 2011].

Besides confined fluids, another emerging area is electrostatic catalysis. Catalysis is one of the most important areas in synthetic chemistry and is traditionally divided between homogeneous and heterogeneous catalysis, usually adopting a molecule or metallic surface as a catalyst [Ramanan et al., 2018]. Alternatively, there has been studies on the application of oriented external electric fields to manipulate reaction rates and control chemical species selectivity through electrostatic catalysis [Shaik et al., 2016].

The direct applications of this technique have great potential in industrial processes [Sequeira and Santos, 2009]. Compared to thermally-based processes, there is the possibility that higher energy efficiency can be obtained with the electrochemical catalysis. It is also conceivable that less expensive materials can be obtained for industrial plants to operate with less severe process conditions. In this scenario, electrostatic catalysis would lead to lower temperatures, decreasing the degradation of the feed and the product. That could

also result in less processing steps, with the possibility to combine reaction and separation inside a reactor, for example.

Furthermore, new process routes could be discovered and change the market share of a product. Still, all of these development is only possible if more investments and studies are made in electrostatic catalysis in the years to come, as it remains one of the less developed areas of synthetic chemistry, despite being widely used in enzymes [Warshel et al., 2006].

The Fischer-Tropsch synthesis (FTS) is potentially a good candidate for electrostatic catalysis in confined systems for consisting of chemical reactions in a heterogeneous catalyst. FTS is the most widely deployed technology in the well-established gas-to-liquids (GLT) process [Papavasileiou et al., 2021]. The GLT process has raised, in the last forty years, as a robust and economically viable route to efficiently produce high quality and environmentally friendly fuels for transportation from natural gas [Wood et al., 2012]. This technology offers a possibility of diversification for natural gas resource holders with the bonus of producing liquid products, which are easier to transport and have a greater energy density. Besides transportation fuel, natural gas can be converted in other drop-in petroleum products. Therefore, FTS is of great interest for the petrochemical industry.

According to the International Energy Agency (IEA), natural gas is already the fastest growing fossil fuel, and in 2020 accounted for 23% of the global primary energy demand and nearly a quarter of electricity generation [IEA, 2021]. There has been 80% of increase in the consumption of the gas between 2010 and 2020, concentrated in three major regions: United States, leaning on the shale gas exploitation, China, due to the increase in the concern about air quality, and Middle East as a way to diversify its oil & gas industry.

Despite this significant growth, the consumption of the gas remains lower them the total capacity. Particularly to the Brazilian case, there was a substantial increase in the amount of natural gas in reservoirs with the pre-salt discoveries in 2006. The options of outflow are, however, still very limited, besides the fact that the economic conditions of the country have been decreasing the internal demand for the gas [dos Santos et al., 2021]. Therefore, the GTL process arises as a possibility to increase the internal demand for natural gas, as well as a possibility to focus on the growing international market for more environmentally friendly petrochemicals and fuels.

In this scenario, Molecular Dynamics simulations were performed to analyse the confined behavior of fluids present in the Fischer-Tropsch synthesis, focusing in the electrostatic catalysis with the application of an static electric field to the system.

1.1 Goals

In this project, we aimed at conducting an exploratory study of the diffusional behavior of confined fluids subject to electrical fields, using Molecular Dynamics simulations, particularly applied in the context of the electrostatic catalysis for the Fischer-Tropsch synthesis.

2 Theoretical background

2.1 Theory and modeling scales

Theory and modeling of systems can be performed at different scales: continuum scale, mesoscale, atomistic level, and electronic level [Gubbins et al., 2011]. From continuum scale to electronic level, the length and time scales naturally decrease as we enhance the level of detail.

The continuum scale description regards the handle of matter as a continuum, in daily-life, observable length and time scales. Matter is not explicitly treated as made of particles and is acknowledged governed by macroscopic laws such as the conservation of matter, energy, and momentum [Gubbins et al., 2011]. The methods using this description can model large physical systems but internal molecular details are disregarded [Mills et al., 2013].

The mesoscale description includes particle-based methods where matter is represented as clusters of molecules or fluid pockets [Mills et al., 2013]. In this scale, the methods can acquire primary aspects of molecular architecture and model, for example, the hydrodynamics of the systems.

On the other hand, at the atomistic level, matter comprehends atoms that follow the laws of classical statistical mechanics [Gubbins et al., 2011]. In this description, molecular architecture and interactions are explicitly modeled. As a result, the analysis only account for small physical domains and diminished scales of time [Mills et al., 2013].

The most detailed method, at electronic level, describes matter as fundamental particles such as electrons and protons, being described by the laws of quantum mechanics [Gubbins et al., 2011]. For such details, this is the most expensive computational method.

Considering computational methods and the availability of supercomputers one can have an idea of the magnitude of these scales [Gubbins et al., 2011]. The density functional theory for example, treating matter at the electronic scale, can easily be used in systems of 100 atoms or more for some tens of picoseconds. Atomistic simulations such as Monte Carlo and Molecular Dynamics can be applied to systems up to billions of atoms,

sizing microns and simulating microseconds of real time. On another hand, with Mesoscale methods, as Brownian and dissipative particle dynamics, one can model larger systems and for numerous orders of magnitude longer, of course losing atomic detail and precision.

In general, despite having a relatively consolidated knowledge of many macroscopic phenomena such as mass and heat transfer, chemical reactions, and phase transition, great development is still needed at molecular or atomic levels [Xiong et al., 2021]. Such a knowledge may lead to a revolution in the future in the way catalysis develops, including reactions in the oil and gas industry. Within this context, Molecular Dynamics simulations are a set of intermediary complexity computational techniques adequate to work on those problems.

2.2 Molecular Dynamics simulations

Historically, computer molecular simulations have been used as a test of theories, and the obtained results compared with the ones of real experiments [Allen and Tildesley, 2017]. In this sense, atomistic computer simulation provides a way to obtain macroscopic properties of a system from the microscopic details, such as the masses of the atoms and the interactions among them. This type of information is of great value for technological advances, since it allows the investigation of conditions that may be difficult, or even unfeasible, to be experimentally studied.

Classical Molecular Dynamics (MD) is a deterministic technique of computer simulation that provides a numerical solution of the classical Newton's equations of motion for a many-body system. From MD results, we are able to compute both equilibrium and transport properties from basic statistical mechanics relations [Frenkel and Smit, 2002].

Molecular Dynamics simulation was originally established by Berni Alder and Tom Wainwright in the 1950s. The first implementation in 1957 examined the phase behavior of hard spheres [Alder and Wainwright, 1957]. Almost a decade later, Aneesur Rahman expanded the method introducing continuous intermolecular potentials to simulate more realistic fluids [Rahman, 1964].

MD consists of some general steps. First, the sample should be prepared by selecting the system. The simulation is initiated by computing the potential energy of all particles based on their positions, velocities, and the interactions among them. From the total

potential energy, the forces acting upon all particles are computed, and Newton's equations of motion are numerically integrated.

The initial configuration usually corresponds to a microstate that does not necessarily belong to the specified thermodynamic condition. Therefore, the initial steps of MD correspond to an equilibration stage. After that, the production stage starts, *i.e.*, from which thermophysical properties can be computed by averaging instantaneous properties over simulation time.

2.2.1 Preparation of the samples

The initial configuration box is built with a certain number of particles in a fixed volume V [Vlugt et al., 2008]. Initial positions $\mathbf{r}_i$ and velocities $\mathbf{v}_i$ are also set for every particle of the system. The positions are assigned in a way that the associated Boltzmann weight is non-zero, which means without hard-core particle overlap. This can be done randomly or placing the particles on lattice sites. Velocities can also be randomly selected within the Maxwell-Boltzmann velocity distribution, considering a specified value of initial temperature, according to the kinetic energy, E_{kin}, definition, as shown in Equation 2.1 [Vlugt et al., 2008].

$$E_{\text{kin}} = \sum_{i=1}^{N} \frac{m{\mathbf{v}_i}^2}{2} = \frac{3Nk_BT}{2}, \tag{2.1}$$

where N is the number of particles, m is the mass of the particles, k_{B} is the Boltzmann constant, and T is the absolute temperature.

Since the simulation is performed in a finite-size box, boundary conditions must be stipulated. A very common boundary condition is the Periodic Boundary Condition (PBC). When PBCs are applied, the system is surrounded by replicas of itself. When referring to a system of particles, this means that if a particle exits the central box in one side, its image will enter in the box on the other side. In this case, the only interaction with that particle to be considered is the one that is closest. This strategy is called nearest image convention [Vlugt et al., 2008], and is illustrated in Figure 2.1.

The application of PBC is needed since there are still a limitation in the number of particles in simulations, still far from the thermodynamic limit. Also, the surface of the box can have an important effect on the properties of the system [Frenkel and Smit, 2002]. In this scenario, PBCs are particularly essential for the particles in the edges of the box to

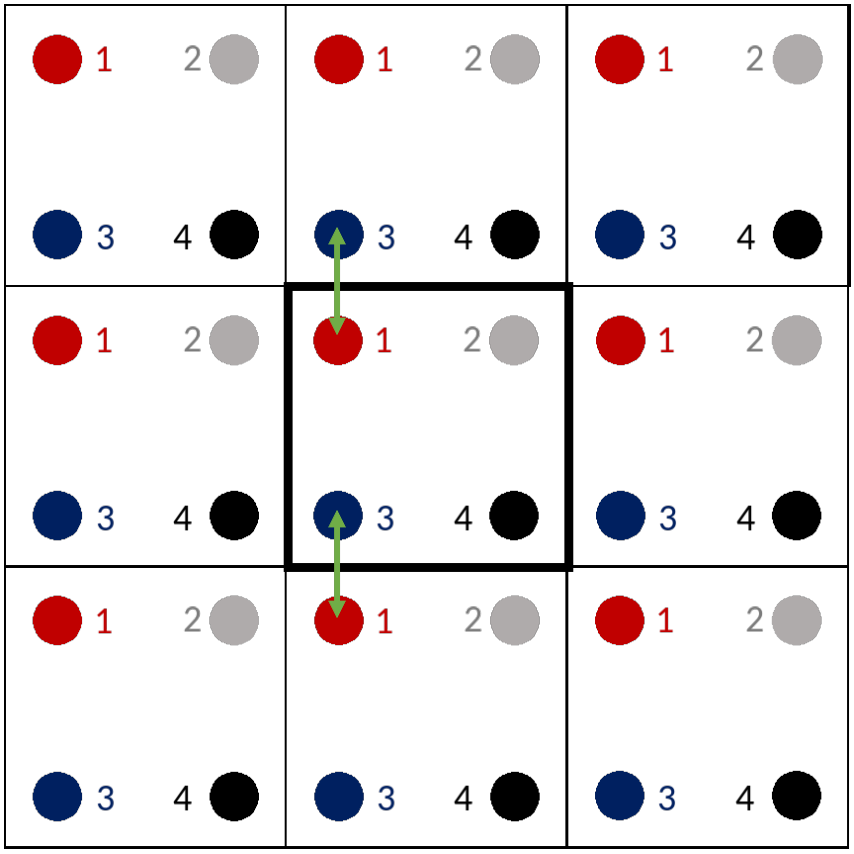

Figure 2.1: Representation of periodic boundary conditions in all directions. The central box is surrounded by replicas of itself. The minimum image convention is represented by the arrows that show the shortest distance between particles 1 and 3.

account for the interactions they would have if an infinite medium was surrounding them.

Consequently, if it is considered only the interaction between the particle and the nearest image of another particle, there are N(N-1)/2 pairs of interactions to be evaluated. To avoid computing a large number of interactions, a cut-off radius, r_{cut}, can be used to limit the distance for which the interactions are computed in less than half the length of the simulation box.

2.2.2 Calculation of total potential energy

The calculation of the forces between molecules or atoms depends on how the interactions between them are described. In Molecular Dynamics, the set of equations used to generate the forces and the parameters to be used in the equations are called force fields [Abraham et al., 2018].

Fundamentally, force field methods rely on the Born-Oppenheimer approximation that nuclear and electronic motions are separable, allowing the energy of a system to be a

function only of the nuclei coordinates. Besides that, another two assumptions involved are: additivity and transferability [Monticelli and Tieleman, 2013]. Additivity implies that a sum of potentials with physical interpretation may be used to account for the total energy of the system. On another hand, transferability assumes that a potential function developed for a narrow number of molecules can be expanded to other molecules that have similarity in chemical groups.

Following that assumptions, for systems represented by more than one particle or atom, nonbonded and bonded interactions need to be accounted for in the total potential function:

$$u_{\text{total}} = u_{\text{nonbonded}} + u_{\text{bonded}}. \tag{2.2}$$

Concerning the nonbonded interactions, it is important to account for the van der Waals forces considering the dispersion interactions and also repulsion caused when atoms overlap [Monticelli and Tieleman, 2013]. For that, the Lennard-Jones (LJ) potential is commonly used in computer simulations. The equation for the LJ potential is represented by Equation 2.3 [Allen and Tildesley, 2017] and graphically illustrated in Figure 2.2:

$$u_{\text{LJ}}(r_{ij}) = 4\varepsilon_{ij}\left[\left(\frac{\sigma_{ij}}{r_{ij}}\right)^{12} - \left(\frac{\sigma_{ij}}{r_{ij}}\right)^{6}\right] = \frac{C_{12}}{{r_{ij}}^{12}} - \frac{C_6}{{r_{ij}}^{6}}, \tag{2.3}$$

where r_{ij} is the Euclidean distance between particles i and j. On another hand, C_{12} and C_6 entail an alternative representation of the potential. Analysing Figure 2.2 it is possible to obtain a better understanding of the other two parameters: σ_{ij} is the distance in which the potential changes sign, ε_{ij} is the potential depth of the attractive well.

Although being a simple expression, LJ potential gives a reasonable description of properties for a series of chemical species provided that the potential parameters, ε_{ij} and σ_{ij}, are chosen properly [Allen and Tildesley, 2017].

When ions are present in the system, or when partial charges are assigned to each particle, LJ potential alone is insufficient to describe the nonbonded interactions, and an electrostatic contribution must be added. Coulomb charge-charge interaction stands out as an alternative. For two particles i and j, the Coulomb potential between them can be calculated as shown in Equation 2.4 [Allen and Tildesley, 2017].

$$u_{\text{Coulomb}}(r_{ij}) = \frac{q_i q_j}{4\pi\epsilon_0 r_{ij}}, \tag{2.4}$$

where q_i is the charge of particle i, and ϵ_0 is the vacuum permittivity.

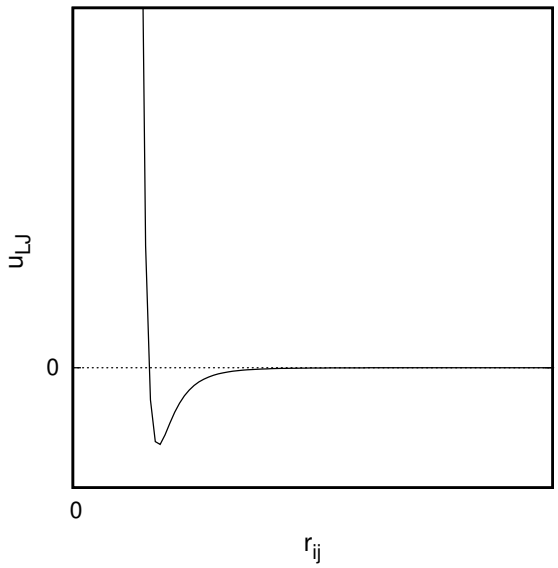

Figure 2.2: General representation of the Lennard-Jones Potential.

For bonded interactions, most cases account for three energy terms: bonds and their deformation (stretching or compressing), angle geometry and bending, and rotation/torsion over dihedral angles [Monticelli and Tieleman, 2013]. In this scenario, the total bonded potential can be computed as shown in Equation 2.5.

$$u_{\text{bonded}} = u_{\text{bonds}} + u_{\text{angles}} + u_{\text{torsions}}. \tag{2.5}$$

Several force fields have been developed over the years. Some of the most used force fields were first developed the 1980's, such as OPLS (Optimized Potentials for Liquid Simulations) focusing on hydrocarbons and applying LJ potential. Originally OPLS used a partially united-atom (UA) model, for which sites for the nonbonded interactions are placed on all atoms but hydrogen atoms attached to aliphatic carbons [Jorgensen et al., 1984]. Latter, the OPLS all-atom representation was developed. Showing explicit hydrogen, this representation grants more flexibility for the distributions of charges and the energetics of torsions [Jorgensen et al., 1996].

The Transferable Potential for Phase Equilibria, TraPPE force field [Martin and Siepmann, 1998], is another example of force fields widely used for hydrocarbons. In TraPPE, the Lennard-Jones potential function is applied. The interaction parameters are also obtained by fitting fluid properties such as critical temperatures and saturated liquid densities.

2.2.3 Integration of Newton's equations of motion

Back to the simulations, after the calculation of total potential energy, the numerical integration of Newton's equations of motion (2.6) can be performed [Gubbins et al., 2011], since the force can be computed from the gradient of the potential energy:

$$\mathbf{F}_i = m_i \mathbf{a}_i = m_i \frac{\mathrm{d}^2 \mathbf{r}_i}{\mathrm{d}t^2} = -\frac{\partial u_{\text{total}}}{\partial \mathbf{r}_i}, \tag{2.6}$$

where $\mathbf{F}_i$ is the force acting upon particle i, m_i is the mass of particle i, and $\mathbf{a_i}$ is the particle acceleration.

Several algorithms can be used to perform the numerical integration, and one of the simplest is the Verlet algorithm. The method is based on a Taylor expansion, resulting in Equation 2.7 for positions [Frenkel and Smit, 2002].

$$\mathbf{r}_i(t+\delta t) \approx 2\mathbf{r}_i(t) - \mathbf{r}_i(t-\delta t) + \frac{\mathbf{F}_i(t)}{m_i}\delta t^2, \tag{2.7}$$

where the estimate of the new position contains an error that is of the order of δt^4, being δt the time step of the simulation.

In this algorithm, the velocity is not used to compute the positions but can be computed according to Equation 2.8 [Frenkel and Smit, 2002].

$$\mathbf{v_i}(t) = \frac{\mathrm{d}\mathbf{r}_i}{\mathrm{d}t} \approx \frac{1}{2\delta t}[\mathbf{r}_i(t+\delta t) - \mathbf{r}_i(t-\delta t)]. \tag{2.8}$$

Another algorithm, based on Verlet's, is the Leap-Frog, used in open source packages such as GROMACS. The velocities are evaluated at half-integer time steps - Equation 2.9 - and used to compute new positions - Equation 2.10 - while Equation 2.11 is used to update the velocities [Vlugt et al., 2008].

$$\mathbf{v_i}\left(t+\frac{1}{2}\delta t\right) = \mathbf{v_i}\left(t-\frac{1}{2}\delta t\right) + \delta t\frac{\mathbf{F_i}(t)}{m_i}, \tag{2.9}$$

$$\mathbf{r_i}(t+\delta t) = \mathbf{r_i}(t) + \delta t\left(t+\frac{1}{2}\delta t\right)\mathbf{v_i}, \tag{2.10}$$

$$\mathbf{v_i}(t) = \frac{1}{2}\left[\mathbf{v_i}\left(t+\frac{1}{2}\delta t\right) + \mathbf{v_i}\left(t-\frac{1}{2}\delta t\right)\right]. \tag{2.11}$$

Being MD a numerical technique, special care must be taken when choosing an appropriate value for the time step, as it has to be small enough to guarantee that

the total energy (E) is conserved during the run, but also large enough to enhance the computational efficiency in sampling the phase space. In the case of flexible molecules, with rapid vibration, this typically requires a time step of about 1 fs [Gubbins et al., 2011].

2.2.4 Ensembles

Due to the conservation of total energy of the system, embedded in the Newtonian description of the motion, the natural ensemble of MD simulations is the microcanonical ensemble, with constant number of particles, volume, and energy (N,V,E). Nevertheless, a lot of properties of interest require constant temperature instead of the total energy, hence the importance to use the canonical ensemble (N,V,T). For that, a thermostat has to be chosen for the system, according to the simulation goal.

To obtain transport properties, some thermostats should be avoided, because they affect the dynamic of the system in a non-continuous way, such as the Andersen thermostat [Andersen, 1980]. Others are more suitable for these properties such as the velocity-rescaling thermostat [Bussi et al., 2007] and the Nosé-Hoover thermostat [Nosé, 1984, Hoover, 1985].

The Nosé-Hoover thermostat first approach was introduced by Nosé [Nosé, 1984] and altered by Hoover [Hoover, 1985]. The equations of motion are extended introducing a thermal reservoir and a friction term. The particles' equations of motion are replaced by Equation 2.12 [Abraham et al., 2018]:

$$\frac{\mathrm{d}^2\mathbf{r}_i}{\mathrm{d}t^2} = \frac{\mathbf{F}_i}{m_i} - \frac{\rho\xi}{Q}\frac{\mathrm{d}\mathbf{r}_i}{\mathrm{d}t}, \tag{2.12}$$

where ξ is a friction parameter (or a heat bath variable). This variable has its own momentum and equation of motion, shown in Equation 2.13:

$$\frac{\mathrm{d}\left(\rho\xi\right)}{\mathrm{d}t} = (T - T_0), \tag{2.13}$$

where T_0 is the reference temperature, and T is the instantaneous temperature of the system.

Back to Equation 2.12, Q is the mass constant of the reservoir and, combined with the reference temperature determine the strength of the coupling. In GROMACS, for exemple, Q is chosen altering the variable τ_t as shown in Equation 2.14:

$$Q = \frac{{\tau_t}^2 T_0}{4\pi^2}, \tag{2.14}$$

where τ_t corresponds to the period of the oscillations of kinetic energy between the system and the reservoir.

Simulations at constant pressure and at constant chemical potential are also possible [Gubbins et al., 2011].

2.2.5 Computing properties

From the trajectory of the system, *i.e.*, the tracking of positions and velocities of the particles over time, macroscopic properties can be computed from statistical mechanical relations. Some examples of the most useful statistical quantities that can be calculated are averages, fluctuations, and correlation functions [Field, 2007].

Averages - Equation 2.15 - and fluctuations - Equation 2.16 - have to be computed over all the configurations that are accessible to the system [Field, 2007]. Temperature, for example, is a property related to the average kinetic energy of a system. Furthermore, heat capacities can be computed from energy fluctuations.

$$\langle X \rangle = \frac{1}{n_t} \sum_{i=1}^{n_t} X_i, \tag{2.15}$$

$$\langle (\delta X)^2 \rangle = \langle (X - \langle X \rangle)^2 \rangle = \langle X^2 \rangle - \langle X \rangle^2, \tag{2.16}$$

where X is the property under consideration, and n_t is the total number of elements in the series.

On the other hand, correlation functions are more complicated to obtain. Auto-correlation functions are described by Equation 2.17, and cross-correlation functions are described by Equation 2.18. From them, transport coefficients, such as diffusion, bulk and shear viscosities, and thermal conductivity, can be computed.

$$\langle \delta X(t) \delta X(0) \rangle = \langle X(t) X(0) \rangle - \langle X \rangle^2, \tag{2.17}$$

$$\langle \delta X(t) \delta Y(0) \rangle = \langle X(t) Y(0) \rangle - \langle X \rangle \langle Y \rangle. \tag{2.18}$$

As computer simulations are usually applied with a pair potential with a spherical cut-off to decrease the number of calculated interactions, the long-range part of the potential that is neglected must be corrected [Allen and Tildesley, 2017]. This correction is

known as tail correction, and represents a factor added to the final values of the properties calculated, such as energy and pressure, for simulations in the canonical ensemble. Tail corrections are only applicable for homogeneous systems, which exclude confined fluids [Franco et al., 2016b].

2.3 Confined fluids

In the last decades, an important field of application of MD simulations have been the investigation of fluids confined in porous materials. As nanotechnology has witnessed an exceptional progress, the importance of understanding nanoscopic systems have been standing out [Heidari et al., 2011]. The study of the behavior of fluids near solid surfaces is essential for several relevant applications in industry such as oil recovery, catalysis, gas storage, and removal of pollutants [Yu et al., 2006].

Fluids confined within porous materials may exhibit drastically different properties compared to the unconfined ones [Qiao et al., 2019]. In fact, at the same temperature, the vapor pressure of pure components in confined spaces is lower than its value for bulk fluids. In addition, the pore radius and capillary pressure considerably affect the critical temperature and pressure of substances [Xiong et al., 2021].

In MD, the studies of confined fluids generally include simple pore geometries, such as cylindrical and slit pores for example, as shown in Figure 2.3. To model these systems, the pore size distribution in real solids are usually disregarded, considering a fixed size value [Qiao et al., 2019].

The properties and the behavior of confined systems are altered as a result of the interaction of the fluid particles with the atoms of the confining walls. These changes emerges in cases where the molecular interaction range and the length scale of the confinement are comparable [Mansoori and Rice, 2014]. The walls in the system influence the energy and the entropy of the confined fluid [Keshavarzi and Kamalvand, 2009]. As a direct result, the local density and the pressure tensor depend on the spatial direction. These are essential elements to describe the thermodynamic state of a system and, therefore, contributes to the differences when compared to bulk fluids [Heidari et al., 2011].

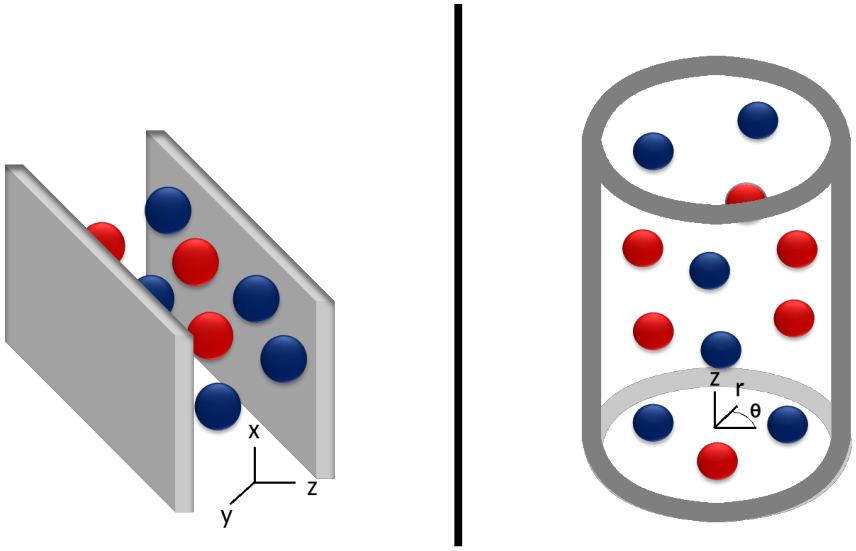

Figure 2.3: Pore geometry: slit nanopore (left) and cylindrical nanopore (right).

2.4 Electrostatic catalysis

Reactions, in general, can be considered as transfer of electrons and/or nuclei, in such manner that it would be expected that kinetics and thermodynamics are influenced by the action of external electric potential [Aragonès et al., 2016]. In fact, electrocatalytic reactions are already applied in industry. Adiponitrile, an intermediate of Nylon, whose process was developed by Monsanto in the 1960s, entails one of world's biggest organic synthesis produced through an electrochemical process [Sequeira and Santos, 2009].

Reactions in the presence of ions, such as the synthesis of adiponitrile, are the ones that most widely uses electrochemical processes. Nevertheless, recent studies have suggested that external electric fields can affect the results of chemical reactions regardless of whether or not an oxidation-reduction system is involved. According to Aragonès et al. [2016], this possibility arises because many formally covalent species can be stabilized through charge-separated resonance hybrids. When an electric field is aligned in such a way to stabilize one of these shapes, the degree of resonance increases, resulting in the complete stabilization of the molecule or transition state. Therefore, a huge scope for application has opened up for this area of expertise.

The experimental demonstration that the Diels-Alder reaction can be catalyzed by an external electric potential [Aragonès et al., 2016] supported the new catalytic approach. The results of the experiment extended the horizons of electrostatic catalysis, as they involve the simultaneous formation of two bonds of carbon-carbon atoms, as

theoretically predicted [Meir et al., 2010]. The proposed theory is that reactivity and regioselectivity (the preference of chemical bonding or breaking in one direction) are fundamentally controllable if the external electric potential is applied in the same axis as the one in which the reaction occurs, since this is the direction in which the electrons are reorganized in the reaction [Shaik et al., 2016]. Nonetheless, stereoselectivity (the preference to form an specific isomer) has a tendency to need a field perpendicular to the reaction axes [Meir et al., 2010].

In this sense, the oriented external electric fields awake ionic structures of bonds that are dormant and result in a dipole orientation. The extent of this phenomenon is a combined result of polarizability of the molecule and the strength of the field [Shaik et al., 2016].

Another promising experimental result was obtained for the reaction of cis-stilbene oxide catalyzed by Al_2O_3 for the formation of diphenylacetaldehyde and 1,3-diphenylacetone. Without the application of an electric field, the selectivity of the reaction was 1:4 for each product, respectively, with the application of the field it was increased to 17:1 [Gorin et al., 2012].

2.5 The Fischer-Tropsch Synthesis

Natural gas is composed mainly of methane and ethane. The conversion of these hydrocarbons to final products through FTS comprise some steps [Wood et al., 2012], illustrated in Figure 2.4. The first one is the production of the synthesis gas (syngas). Initially occurs the separation and reconfiguration of carbon and hydrogen of the alkanes by steam reforming or partial oxidation. The products of this step are primarily carbon monoxide and hydrogen.

Next, the FTS step takes place. This reaction may be performed in fixed-bed, fluidized-bed or slurry bubble-column-type reactors depending on the core technology [van de Loosdrecht et al., 2013]. This is a highly exothermic polymerization reaction [Papavasileiou et al., 2016] to produce synthetic liquid hydrocarbons (synthetic crude or syncrude), mostly long-chain paraffin with as many as 100 carbons in a molecule [Wood et al., 2012]. The principal reaction of this step is:

$$\mathrm{nCO} + (2\,\mathrm{n} + 1)\,\mathrm{H_2} \longrightarrow \mathrm{H(CH_2)_nH} + \mathrm{nH_2O}$$

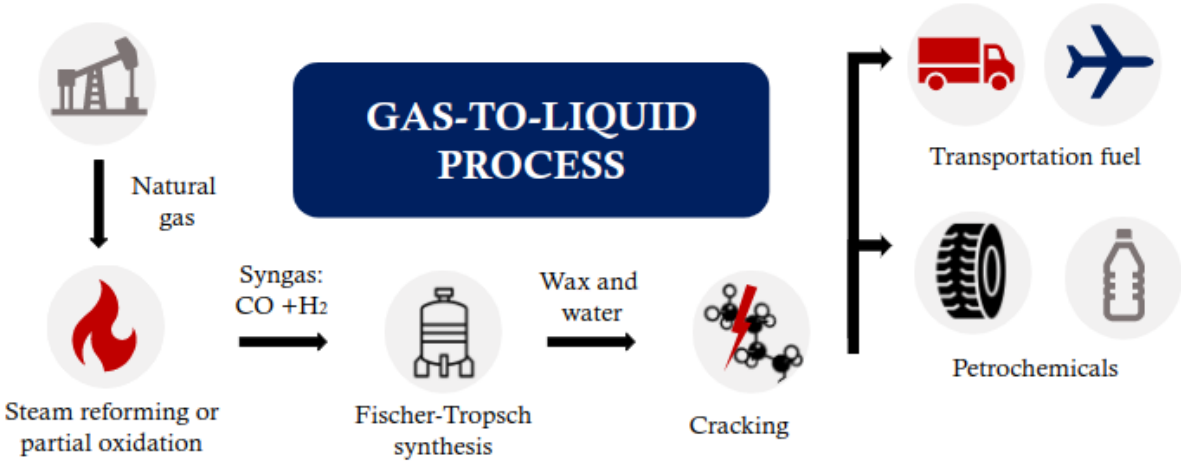

Figure 2.4: Representation of the gas-to-liquid process.

The obtained liquid hydrocarbon is also known as wax due to the similarity in appearance to wax at room temperature. Water and a small amount of oxygenated compounds, such as alcohols, are also products of the reaction [Papavasileiou et al., 2021].

The last step of the GTL process consists of cracking the molecules. The process can be carried out in crackers such as those of conventional refineries, and can be modulated depending on the demand of the market [Wood et al., 2012].

The focus of this work is related to the Fischer-Tropsch synthesis step, which has already been applied commercially. As in any synthesis, it is essential to work on optimizing catalyst activity and selectivity [Papavasileiou et al., 2016]. As a result, the choice of the active material is critical. Nowadays, Co and Fe are the ones more suitable for industrial applications [van de Loosdrecht et al., 2013].

The operating conditions of the reactors are also of paramount importance. The process can be done at high temperature, HTFT, reaching values between 573 and 623 K, or at low temperature, LTFT, working in the interval 473-513 K. Cobalt is essentially only applied in LTFT process due to its high yield to produce linear long-chain paraffin, stability, and resistance to deactivation [Khodakov et al., 2007]. Shell applies the Co LTFT technology in plants in Malaysia and Qatar, using fixed-bed reactors [van de Loosdrecht et al., 2013].

The catalyst support has also a relevant role in the synthesis, mostly regarding surface structure and pore size [Khodakov et al., 2007], influencing CO conversion, selectivity, and diffusion coefficients of reactants and products [Jahangiri et al., 2014]. Typically, metal oxides such as aluminium oxide (Al_2O_3), silicon dioxide (SiO_2), and titanium dioxide

(TiO_2) are the ones employed in this synthesis [Oh et al., 2009].

Graphene and its derivatives have recently been studied in catalysis as a result of its exceptional physical properties, which include the possibility to be used both as support or as metal-free catalysts [Karimi et al., 2015, Hajjar et al., 2017, Papavasileiou et al., 2021]. The material was originally isolated from graphite as single-layer graphene or few-layer graphene as a sp_2 hybridized carbon material [Karimi et al., 2015].

Graphene's based catalyst unique structure leads to high specific surface area, high adsorption capacity, chemical and electrochemical inertness, and simple surface modification [Machado and Serp, 2012]. Furthermore, limitations of internal mass transfer in the reactions are much smaller than traditional supports, whereas being very stable and quite recyclable.

For Fischer–Tropsch synthesis, the compounds most widely considered entail pristine graphene (G) and graphene oxide (GO) [Papavasileiou et al., 2021]. Experiments of Cobalt FTS using graphene and graphene oxide as a support showed an increase in CO conversion and a better catalyst stability when compared with the traditional supports [Karimi et al., 2015, Hajjar et al., 2017]. Compared to Al_2O_3, for instance, the increment in conversion for graphene reached 85%, besides higher selectivity for linear long-chain hydrocarbons [Karimi et al., 2015].

Among several possible analyses of this system there is MD. Molecular Dynamics simulations based on graphene and graphene oxide supports have been reported by Papavasileiou et al. [2021]. This particular referred work focuses on studying the phase behavior of the main products of the reactions, the mixture wax-water, accounting for confinement effects. One of the calculated parameters was self-diffusion, which was accurately captured as a function of the distance from the pore center, being lower closer to the pore surface.

2.6 Diffusion

Diffusion is one initial aspect to study the overall behavior of the reaction in nanopores. At the macroscopic scale, diffusion represents the transport of matter in a system from one part to another [Crank, 1975], and is of fundamental importance for several natural and industrial processes. Mass transfer processes in the chemical industry

are frequent, and often represent the limiting step of the operation [Santos et al., 2021]. Attempts to try to describe mathematically mass diffusion started in 1855 with the German physician Adolf E. Fick. What latter came to be known as Fick's law of diffusion is still the most commonly used method in continuum scale modeling [Gubbins et al., 2011].

As for other equations derived for transport phenomena, as well as for Newton's law for momentum and Fourier's law for heat transfer, Fick's law belongs to the linear phenomenological models, for which the flux is proportional to a driving force. For Fick's law, the driving force is taken as the concentration gradient. The factor of proportionality between the flux and the driving force in diffusion is the diffusion coefficient [Franco et al., 2016b].

In fact, the diffusion observed by Fick is now recognized to be a result of a chemical potential gradient in the system instead of concentration. The macroscopic event leads to a mass flow of each component increasing the entropy of the medium as it moves to equilibrium [Santos et al., 2021]. A simpler form of diffusion is self-diffusion that includes molecular diffusion as a result of collisions and the random Brownian motion above absolute zero (0 K) in uniform fluids.

Temperature and pressure of the medium have a great impact in diffusion coefficients. Industrial processes that take place in large ranges of temperature, pressures, and concentration face serious challenges as experimental measurements for every condition are unfeasible. Predictions of this transport property are difficult to make, but several approaches have been studied mostly regarding semi-empirical correlations [Santos et al., 2021].

To obtain the self-diffusion coefficient, D, it is necessary to relate it with the trajectory of the particles. Two main approaches have been used to compute the self-diffusion coefficients from MD trajectories. In the first one, derived by Einstein, the mean-square displacement (MSD) of the molecules are computed as a function of time, $\langle r^2(t)\rangle$, and related to D [Frenkel and Smit, 2002] as shown in Equation 2.19:

$$D = \lim_{t\to+\infty} \frac{1}{2d} \frac{\partial\langle r^2(t)\rangle}{\partial t}, \tag{2.19}$$

where d denotes the dimensionality of the system.

Although D is a macroscopic coefficient, the MSD can be understood microscopically computing the square of the distance traveled by every particle i in time t, and averaging

over the number of particles, N, as shown in Equation 2.20:

$$\langle \Delta r(t)^2 \rangle = \frac{1}{N} \sum_{i=1}^{N} \Delta \mathbf{r}_i(t)^2. \tag{2.20}$$

Another approach starts from Einstein's relation, and expresses the diffusion coefficient in terms of the time integral of the autocorrelation function of the velocity $\mathbf{v_i}$, which is a Green-Kubo relation [Liu et al., 2004]:

$$D = \frac{1}{d} \int_0^\infty \langle \mathbf{v}_i(t) \cdot \mathbf{v}_i(0) \rangle \mathrm{d}t. \tag{2.21}$$

Both approaches are derived from Fick's diffusion equation and consider free boundary conditions, which apply exclusively to calculations in homogeneous fluids [Liu et al., 2004]. Therefore, when a heterogeneity emerges in the system, such as a density gradient, the diffusion coefficient needs to be considered a tensor instead of a scalar [Franco et al., 2016a]. That heterogeneity can be caused, for example, by the presence of a wall in the system, as it happens for confined fluids.

Since transport properties are difficult to predict or to measure experimentally even in bulk systems, there is an extra challenge when confined fluids are considered. Therefore, MD simulations play a fundamental role in predicting these properties. In confined fluids, the MSD will be restricted to the size of the nanopore such that molecules stay in the region of interest just for a finite time. As a result to that, there may be different diffusion coefficients for each region and the time dependence of MSD will became linear only if there is enough time to sample all regions [Liu et al., 2004].

For confined systems, a more appropriate description of the particle distribution is based on the Smoluchowski equation - Equation 2.22:

$$\frac{\partial p(\mathbf{r},t)}{\partial t} = \boldsymbol{\nabla} \cdot \mathbf{D} e^{-\beta W(\mathbf{r})} \cdot \boldsymbol{\nabla} \left[e^{\beta W(\mathbf{r})} p(\mathbf{r},t) \right], \tag{2.22}$$

where $p(\mathbf{r},t)$ is the probability density function, $\mathbf{r}$ the position vector, $\mathbf{D}$ the diffusion tensor, $\beta = 1/(k_\mathrm{B}T)$. Moreover, $W(\mathbf{r})$ is the potential of the mean force that is related to the correlation function:

$$e^{-\beta W(\mathbf{r})} = g(\mathbf{r}) = \frac{\rho(\mathbf{r})}{\langle \rho \rangle}, \tag{2.23}$$

where $\rho(\mathbf{r})$ is the particle density distribution, and $\langle \rho \rangle$ is the average density.

In confined systems such as a slit pore, the diffusion tensor is orthogonal to the plane of the interface, in this case z, which may be defined as the perpendicular component whereas the other two, x and y, are the parallel components.

A methodology to compute the parallel components in inhomogeneous systems was proposed by Liu et al. [2004]. The approach was to divide the system in thin layers parallel to the interface and study each layer Ω individually, applying the Smoluchowski approach - Equation 2.22. The coefficients vary from layer to layer, especially near to the surface, but are not expected to vary inside them. The result of this method is shown in Equation 2.24:

$$D_{\parallel} = \lim_{t\to\infty} \frac{\langle \Delta r^2(t) \rangle_{\Omega}}{2tP(t)}. \tag{2.24}$$

The mean-square displacement in this case captures the motion of particles within each layer between a time t_0 and $t + t_0$, taking different time origins and averaging over τ steps as shown in Equation 2.25:

$$\langle \Delta r^2(t) \rangle_{\Omega} = \frac{1}{\tau} \sum_{t_0=0}^{\tau-1} \frac{1}{N(t_0)} \sum_{i\in\Omega(t_0,t_0+t)} (\mathbf{r}_i(t_0+t) - \mathbf{r}_i(t_0))^2. \tag{2.25}$$

The survival probability - Equation 2.26 - is the ratio between the number of particles remaining in the layer after a certain time, $N(t, t+t_0)$, and the number of particles computed at the initial time, $N(t_0)$, disregarding possible re-entrance due to the virtual boundary condition.

$$P(t) = \frac{1}{\tau} \sum_{t_0=0}^{\tau-1} \frac{N(t_0,t_0+t)}{N(t_0)}. \tag{2.26}$$

Regarding the perpendicular component of self-diffusion, numerous methods have been proposed in the literature [Liu et al., 2004, Mittal et al., 2008, Franco et al., 2016b]. The methodology developed by Franco et al. [2016b] can be applied to both homogeneous and inhomogeneous systems. The coefficient is determined from the analytical solution of the Schmoluchowski equation for a linear potential of mean force by integrating the survival probability.

The calculation is applied for each layer of the system, considering it is thin enough for the diffusion coefficient to be taken as a constant. Therefore, the Schmoluchowski equation for a perpendicular component z, can be written as:

$$\frac{\partial p(z,t)}{\partial t} = D_{\perp} \left[\frac{\partial^2 p(z,t)}{\partial z^2} + \frac{\partial}{\partial z} \left(p(z,t)\beta \frac{\partial W(z)}{\partial z} \right) \right]. \tag{2.27}$$

Assuming that the solution to the time-dependent second order partial differential is separable in terms of time and space, and applying further mathematical manipulation,

Equation 2.28 can be used for computing the perpendicular component of self-diffusion:

$$D_{\perp} = \frac{L^2}{\alpha \tau_r}, \tag{2.28}$$

where L is the layer width, and τ_r, as shown in Equation 2.29, is defined as the integral of the survival probability - Equation 2.30:

$$\tau_r = \int_0^{+\infty} P(t)\mathrm{d}t, \tag{2.29}$$

$$P(t) = \int_0^{L} p(z,t)\mathrm{d}z. \tag{2.30}$$

The assumption that the layer Ω should be small enough so that diffusion coefficient may be considered independent of the position has further consequences. One of them is reasonably assuming that, in such a small layer, the potential of mean force may be estimated by a linearization of Equation 2.23 in direction z:

$$-\beta W(z) = \ln\left[\frac{\rho(z)}{\langle\rho\rangle}\right] = \omega z + \xi, \tag{2.31}$$

where ξ is the linear coefficient.

From Equation 2.31, as the potential of mean force is considered linear, so is the natural logarithm of the equilibrium density:

$$\ln\left[\frac{\rho(z)}{\rho^*}\right] = \omega z + \xi', \tag{2.32}$$

where $\xi' = \xi + \ln(\langle\rho\rangle/\rho^*)$, $\rho(z)$ is the mass density distribution in kg·m^3 and $\rho^* = 1.0$ kg·m^3, a normalization parameter.

In this scenario, the Schmoluchowski equation for z, can be rewritten as:

$$\frac{\partial p(z,t)}{\partial t} = D_{\perp}\left[\frac{\partial^2 p(z,t)}{\partial z^2} - \omega\frac{\partial p(z,t)}{\partial z}\right]. \tag{2.33}$$

Applying further mathematical manipulation, the analytical solution to Equation 2.33, for $\omega < 2\pi/\mathrm{L}$, is:

$$p(z,t) = \frac{2\pi\omega}{L^2(e^{\omega L}-1)}\sum_{\mathrm{n}=1}^{+\infty}\frac{n\left[1-e^{\omega L}\cos(n\pi)\right]}{\left(\omega^2+\frac{n^2\pi^2}{L^2}\right)} \times \sin\left(\frac{n\pi z}{L}\right)\exp\left[-\left(\frac{n^2\pi^2}{L^2}-\frac{\omega^2}{4}\right)D_{\perp}t\right]. \tag{2.34}$$

The survival probability, as the integral in space of Equation 2.34, is given by:

$$P(t) = \frac{4\omega}{L}\frac{(e^{\omega L}+1)}{(e^{\omega L}-1)}\sum_{\mathrm{j}=0}^{+\infty}\frac{\exp\left[-\left(\frac{(2j+1)^2\pi^2}{L^2}\right)D_{\perp}t\right]}{\left(\omega^2+\frac{(2j+1)^2\pi^2}{L^2}\right)}. \tag{2.35}$$

The residence time, on another hand, is computed from Equation 2.29 as:

$$\tau_r(t) = \frac{4\omega}{D_\perp L}\frac{(e^{\omega L}+1)}{(e^{\omega L}-1)}\sum_{\mathrm{j}=0}^{+\infty}\frac{1}{\left(\frac{(2j+1)^2\pi^2}{L^2}-\frac{\omega^2}{4}\right)\left(\omega^2+\frac{(2j+1)^2\pi^2}{L^2}\right)}. \tag{2.36}$$

Back to Equation 2.28, α is given by:

$$\alpha^{-1} = 4\omega L\frac{(e^{\omega L}+1)}{(e^{\omega L}-1)}\sum_{\mathrm{j}=0}^{+\infty}\left[(2j+1)^4\pi^4+\frac{3\omega^2L^2}{4}(2j+1)^2\pi^2-\frac{\omega^4L^4}{4}\right]^{-1}. \tag{2.37}$$

For homogeneous systems, $\omega \to 0$ as a result to the potential of the mean force being independent of the position. Therefore, $\alpha = 12$ [Franco et al., 2016b].

The choice of the size, L, and position of layer Ω is arbitrary when applying the methodology of Franco et al. [2016b], as long as the potential of mean force can be considered linear. The study of Spera et al. [2022], in which the author took part, evaluates how the choice of some of this arbitrary parameters can influence the results of the self-diffusion coefficient.

The systems that Spera et al. [2022] studied contained methane, ethane or their mixtures, besides CO_2. Particularly, there was the evaluation of the effect of the choice of the layer interval in the self-diffusion coefficients. For the systems studied, the results shows that the values of the coefficient differ depending on the size of the interval chosen, specially for $D_\perp$. The general recommendation obtained from the article's results is that the same boundary values should be chosen for both $D_\parallel$ and $D_\perp$ to properly analyse the results. Of course this choice should be done based on the density profile.

3 Methodology

3.1 Simulation details

The system chosen as representative of the Fischer-Tropsch synthesis was the product of the reaction: hydrocarbons and water, confined in a slit pore of graphene sheets, with 5 layers in each side of the pore of 5.88 nm of width [Papavasileiou et al., 2021]. The hydrocarbons selected were methane, *n*-butane, and *n*-pentane.

The composition of the mixtures studied were calculated based on the stoichiometry of the FTS reaction and assumes a 1:1 H_2O : CH_x(x = 2 or 3) ratio in the pore. The codes used to perform the computer simulations were PACKMOL (initial configuration) and GROMACS (Molecular Dynamics). Gnuplot was used for plotting graphics, and VMD for the visualization of the system.

PACKMOL [Martínez et al., 2009] is a software package, written in Fortran, that creates a starting point for Molecular Dynamics by packing molecules into defined regions of space. This step is import to ensure that short-range repulsive interactions do not disrupt the simulation. The user must enter only the initial coordinates of the simulation box and the number of molecules, in addition to the spatial restrictions that each type of molecule must satisfy.

With the initial configuration provided by PACKMOL from the specifications of the molecules of the system, GROMACS can be used to numerically integrate the Newtonian equations of motion. GROMACS [Abraham et al., 2018] is a versatile package for performing MD for hundreds to millions of particles. The version that was used was GROMACS 2021.2.

Initially, one sheet of graphene was created based on a sort of unitary cell of 4 atoms of carbon, forming half of regular hexagon with an angle of 120° between the atoms, as show in Figure 3.1.

Next, the coordinates of the atoms were replicated in axes x, y, and z respectively 19, 11 and 1 times, resulting in one layer of 836 atoms of carbon. This was done using the *gmx genconf* tool of GROMACS. The result can be seen in Figure 3.2

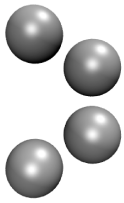

Figure 3.1: Representation of carbon atoms to form a sheet of graphene.

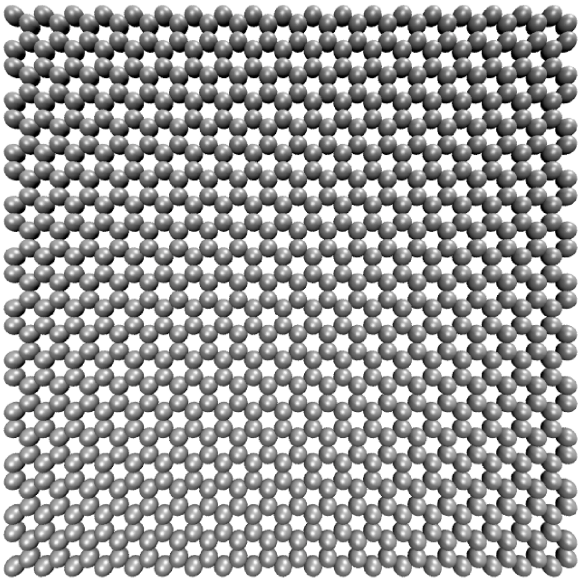

Figure 3.2: Atomistic model for a single-layer graphene sheet.

To build the total structure of the slit pore PACKMOL was used, consisting of two blocks of five Bernal-stacked multilayer graphene [Rao et al., 2009]. The distance used between the layers in the same block was 3.48 Å. Moreover, in this kind of block, the multilayers are not perfectly aligned, instead they present a displacement of 0.14 nm between them, as represented in Figure 3.3.

The steepest descent method was used with a maximum number of iterations equal to 50000 to relax the initial multilayer graphene. To prevent an undesired displacement between the graphene sheets, a position restrain file was created using the *gmx genrestr* command with force constants of 1000 $kJ \cdot mol^{-1} \cdot nm^{-2}$ in all directions. The imposed position restrain allows fixing the graphene atoms in the position of the beginning of the simulation.

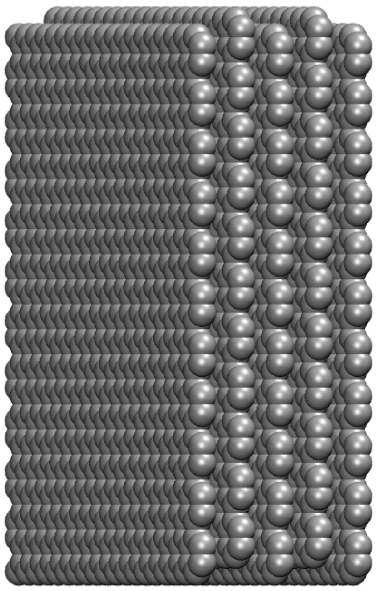

Figure 3.3: Atomistic model for a five-layer graphene structure.

The mixtures of hydrocarbons and water were created with PACKMOL in a box of size 46.0725 × 47.6 × 53.2 Å. Then, they were confined between the slit pores using a code in C language enlarging the pore diameter in 0.2 Å in the z direction. This action was also necessary to ensure graphene atoms stay fixed. The initial configurations and the codes used in this work are available in a github page: https://github.com/Flavianbraga/Codes-for-dissertation.

The number of water molecules were fixed in 1680 for all the systems. Regarding the hydrocarbons, for methane the number of molecules was 1680, for n-butane was 420 and for n-pentane 336.

Prior to the MD simulation, the steepest descent method was used with a maximum number of iterations equal to 50000 to relax the initial configuration. Then, an equilibration step was performed in the canonical ensemble for 20 ns, followed by 40 ns of production steps in the same ensemble. The simulations were performed in the canonical ensemble to fix the temperature and the pore size.

The numerical integration was done using the Leap-Frog algorithm with a time step of 1 fs. Positions and velocities were stored every 0.2 ps. Nosé-Hoover thermostat was used to keep the temperature of the entire system at 573.15 K, with the period of the temperature fluctuations at equilibrium of $\tau_{\mathrm{T}} = 0.5$ ps.

Graphene and the hydrocarbons were modeled by the OPLS-AA force field [Jor-

gensen et al., 1996]. The presence of explicit hydrogen and the flexibility obtained for the distribution of charges and torsional energetics are specially relevant aspects when considering the influence of an applied electric field such as in this study.

The OPLS-AA model accounts for the interaction between carbon atoms according to the structure of the molecules. The ones presented in this work are : CH_4, present in methane, CH_3 and CH_2 present in *n*-butane and *n*-pentane, and ca present in graphene. In this study, there is a specific site for graphene, ca, that is modeled according to Jorgensen et al. [1996] as the atoms of naphthalene. For the hydrogen atoms, the parameters are the same regardless of the molecule of the hydrocarbon.

Water was represented by the rigid TIP4P/2005 model [Abascal and Vega, 2005]. This force field has proven to be notably accurate to predict water properties, especially self-diffusion [Vega and Abascal, 2011]. The determination of the dielectric constant is also of great interest, because it measures the response of the water molecules under the effect of an electric field. This property is reasonably represented by TIP4P/2005, with the best results among nonpolarizable force fields [Aragones et al., 2011].

In the TIP4P/2005 model, there are four interaction sites: one in each atom of the H_2O molecule, and another one, the BE site, which is coplanar with the oxygen and hydrogen atoms placed at the bisector of the H-O-H angle [Abascal and Vega, 2005]. A single Lennard-Jones interaction site is accounted for at the oxygen atom, uncharged, while electrostatic positive charges are present at the hydrogens and the negative charge is placed in the BE site.

In both cases, the Lennard-Jones potential function is applied (Equation 2.3). The parameters taken from these studies [Jorgensen et al., 1996, Abascal and Vega, 2005] are reported in Table 3.1.

The LJ parameters for the interaction between the fluids and between the fluids and the wall were calculated applying geometrical combining rules as shown in Equations 3.1 and 3.2:

$$\sigma_{ij} = \left(\sigma_{ii}\sigma_{jj}\right)^{1/2}, \tag{3.1}$$

$$\varepsilon_{ij} = \left(\varepsilon_{ii}\varepsilon_{jj}\right)^{1/2}. \tag{3.2}$$

Regarding bonded interactions, the intramolecular potentials include bonds, angles,

Table 3.1: Non-bonded parameters.

Atom or group	Mass (g·mol^{-1})	σ (Å)	ϵ (J· mol^{-1})	Charge (e)
H,alkanes	1.0080	2.5000	0.125520	0.0600
C,CH_4	12.0110	3.5000	0.276144	−0.2400
C,CH_3	12.0110	3.5000	0.276144	−0.1800
C,CH_2	12.0110	3.5000	0.276144	−0.1200
ca,Graphene	12.0110	3.5500	0.292880	0.0000
H,Water	1.0080	0.0000	0.000000	0.5564
O	15.9994	3.1589	0.774910	0.0000
BE	0.0000	0.0000	0.000000	−1.1128

and torsions. For the OPLS-AA force field bond stretching is represented by Equation 3.3 and the parameters are presented in Table 3.2:

$$u_{\text{bonds}} = \sum_{\text{bonds}} K_{\text{bond}}(r_{ij} - r_{\text{eq}})^2, \tag{3.3}$$

where K_{bonds} is the force constant, and r_{eq} is the equilibrium distance.

For water, bond lengths between atoms O-H were fixed as 0.09572 nm. To keep bonds fixed, when applied, LINCS constraint algorithm [Hess et al., 1997] was used.

Table 3.2: Bonded parameters for bonds.

Bond Type	Bond Length/r_{eq}(nm)	K_{bond} (kJ · mol^{-1}· nm^{-1})
H−C	0.1090	284512.0
C−C	0.1529	224262.4
ca−ca	0.1400	392459.2

For OPLS-AA, angle bending is expressed in Equation (3.4), where θ_{ijk} is the angle between 3 atoms i, j, and k.

$$u_{\text{angles}} = \sum_{\text{angles}} K_\theta(\theta_{ijk} - \theta_{\text{eq}})^2. \tag{3.4}$$

The parameters are presented in Table 3.3. For water the angle is fixed in 104.52°.

The torsion potential is a function of Fourier dihedral angles, ϕ. In GROMACS, in order to obtain a more efficient calculation, this bonded parameter is described by Equation 3.5.

$$u_{\text{torsions}} = \frac{1}{2}C_1[1 + \cos\phi] + C_2[1 - \cos(2\phi)] + C_3[1 + \cos(3\phi) + C_4[1 - \cos(4\phi)]. \tag{3.5}$$

Table 3.3: Bonded parameters for angles.

Angle type	Angle/θ_{eq}(deg)	K_θ (kJ· mol^{-1})
C−C−H	110.7	313.800
H−C−H	107.8	276.144
C−C−C	112.7	488.273
ca−ca−ca	120.0	527.184

The parameters used in GROMACS, C_0 to C_4, are translated to Ryckaert-Bellemans parameters from the original OPLS-AA referece [Jorgensen et al., 1996], F_1 to F_4, which can be related as:

$$C_0 = F_2 + \frac{1}{2}(F_1 + F_3), \tag{3.6a}$$

$$C_1 = \frac{1}{2}(-F_1 + 3F_3), \tag{3.6b}$$

$$C_2 = -F_2 + 4F_4, \tag{3.6c}$$

$$C_3 = -2F_3, \tag{3.6d}$$

$$C_4 = -4F_4. \tag{3.6e}$$

The OPLS-AA original parameters are presented in Table 3.4 while Ryckaert-Bellemans parameters are presented in Table 3.5 .

Table 3.4: OPLS-AA bonded parameters for dihedrals in kcal· mol^{-1}.

Dihedral type	F_1	F_2	F_3
C−C−C−C	1.740	−0.157	0.279
C−C−C−H	0.000	0.000	0.366
H−C−C−H	0.000	0.000	0.318
ca−ca−ca−ca	0.000	7.250	0.000

The nonbonded interactions were computed based on a neighbor list; a list of non-bonded particles in a certain radius. Neighbor searching was performed with the Verlet cut-off scheme up to the distance of 1.4 nm and the grid research type was used.

Table 3.5: Ryckaert-Bellemans bonded parameters for dihedrals in kJ· mol^{-1}.

Dihedral type	C_0	C_1	C_2	C_3	C_4
C−C−C−C	2.92880	−1.4644	0.20920	−1.67360	0.00000
C−C−C−H	0.62760	1.88280	0.00000	−2.51040	0.00000
H−C−C−H	0.62760	1.88280	0.00000	−2.51040	0.00000
ca−ca−ca−ca	30.33400	0.00000	−30.334	0.000000	0.00000

To compute electrostatic Coulombic interactions, Particle Mesh Ewald method [Darden et al., 1993] was used. The distance applied for the cut-off was 1.4 nm.

Regarding the application of an electric field in a system for MD simulations, two approaches were analysed. The first one is more straightforward to be implemented in GROMACS, defining the amplitude of the electric field as an input and simulating the system [Wei et al., 2005, Tang et al., 2004]. The total force of the system is changed adding a component of the form of the Equation 3.7:

$$\mathbf{F}_{\text{ext}} = \mathbf{q_i}\mathbf{E}_{\text{field}}, \tag{3.7}$$

where q_i is the charge of particle i, and $\mathbf{E}_{\text{field}}$ is the applied electric field.

The fields applied in GROMACS were static and of magnitude 0.0, 1.5, 3.0, 4.5, 6.0, 7.5 V/nm for comparison, only in the z direction, taking Figure 3.4 as reference for the axes. Due to the arrangements made in the system to apply the electric field, no Periodic Boundary Condition in the z axis can be applied. Therefore, PBC were applied only in directions x and y. For that, the walls for both sides need to be present in the initial configuration.

The second approach [Elabyouki et al., 2019, Fiates et al., 2020] consists of adding charges to the graphene atoms in the layer in contact with the fluid, balancing positive charges in one side and negative charges in the opposite side. Therefore, an electric field is induced.

In this study, the charges were distributed homogeneously in the surface, adding $0.013158e$ to each of the 836 atoms, resulting in $11e$ or $17.62{\cdot}10^{-19}$ C. The net charge, however, is zero.

Theoretically, pure water molecules suffer electrolysis in voltages above than 1.23 V [Kim et al., 2019]. To observe in a different behavior of the molecules, however, higher values had to be used, as in other related studies, to amplify the response signal. When

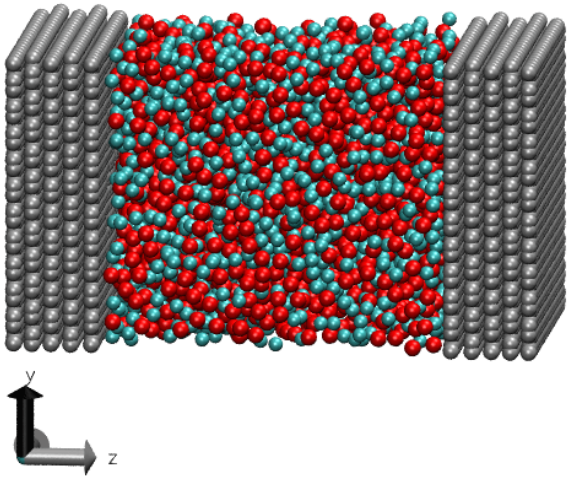

Figure 3.4: Initial configuration of the mixture of water (cyan) with methane (red) in a slit pore of graphene (silver) as a reference for the axis representation.

considering the gradient of parameters in confined media, this is a common approach to obtain analysable results. For example, in gas/oil reservoirs simulations, an unrealistic thermal gradient of close to $3{\cdot}10^{10}$ K·m^{-1} is used [Spera and Franco, 2021].

3.2 Simulation Analysis

To further understand the results of the simulations, some analysis were performed. First, to compute the density profile of the system. For that, the GROMACS command *gmx density* was used in all directions (x, y, z) for each component methane, n-butane, n-pentane, and water in their respectively mixtures. The results were averaged in time in each of the 1000 slabs in which the box was divided in the z direction.

Another analysis was the order parameter. The order parameter is related to the orientation of the molecules. For water, the calculation done in this study is based on the angle α between the dipole moment of the molecule and the axis z. A code in C language is used to divide the box in slices and calculate the average orientation per slice in the time of the simulation.

The order parameter (S) is obtained using Equation 3.8:

$$S = \frac{(3 \cdot \cos\alpha^2 - 1)}{2}. \tag{3.8}$$

The value for the cosine of α is computed dividing the inner product of the vector corresponding of the dipole moment (x_{dm}, y_{dm}, z_{dm}) and the vector normal to the surface

z (0, 0, 1) by the product of the length of those vectors as shown in Equation 3.9:

$$\cos\alpha = \frac{(x_{dm}\cdot 0 + y_{dm}\cdot 0 + z_{dm}\cdot 1)}{\sqrt{(x_{dm}^2 + y_{dm}^2 + z_{dm}^2)\cdot(0^2+0^2+1^2)}}. \tag{3.9}$$

As will be discussed latter, due to the results of the system, the calculation of the self-diffusion coefficient was not possible. The survival probability, however, was still computed for the systems using Equation 2.26 with multiple time origins. The calculation was one done in the center of the pore and the interval chosen for the layer was from 4.25 to 4.75 nm.

4 Results and discussion

4.1 Qualitative analysis

The first conducted analysis of the simulated systems is a qualitative visual inspection. The initial configuration of the systems was the same for all electric fields applied and is represented in Figure 4.1 for methane, *n*-butane, and *n*-pentane. All simulations were carried out at 573.15 K. which is compatible to the operation condition of Fischer-Tropsch synthesis.

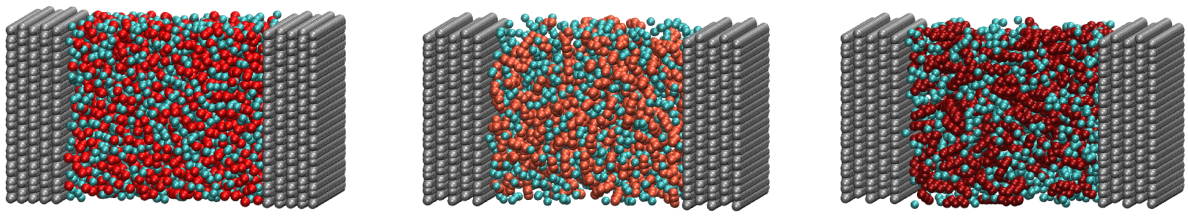

(a) Methane **(b)** *n*-Butane **(c)** *n*-Pentane

Figure 4.1: Atomistic representation of the initial configuration of systems containing water (cyan) mixtures with methane (red), *n*-butane (orange), and *n*-pentane (dark-red) in a slit pore of graphene (silver).

Two approaches for the application of the field were analysed. First, the cases using the direct GROMACS input of the magnitude of the electric field will be presented. The final configurations of the mixture water/methane are shown in Figure 4.2. For *n*-butane, the results are in Figure 4.3 whereas for *n*-pentane the results are in Figure 4.4.

For methane, *n*-butane, and *n*-pentane, the results are very similar for each applied electric field. For the two lower values of the field, water is contained at the center of the pore while the hydrocarbons concentrate near the wall. This is expected since graphene is a hydrophobic surface. This behavior changes with the increase of the electric field. For 3 V/nm, the phase separation starts to occur in a different direction. For higher values, this separation is not completely clear from this point of view and seems to occur more randomly. Consequently, to get a deep understanding of this behavior, it is important

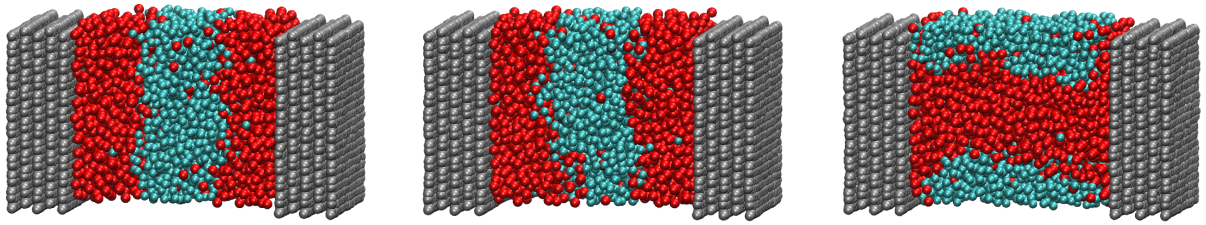

(a) 0.0 V/nm **(b)** 1.5 V/nm **(c)** 3.0 V/nm

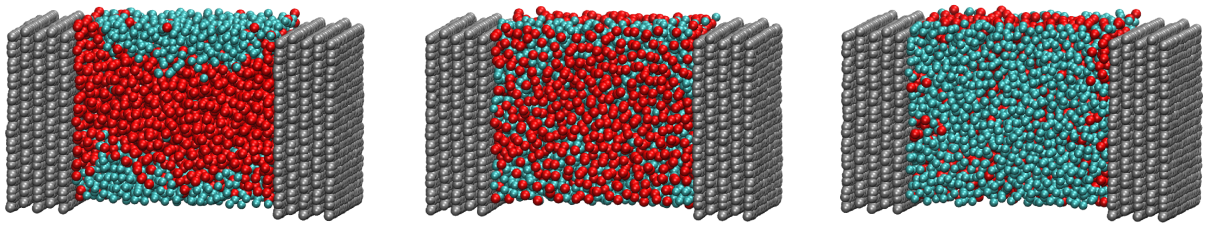

(d) 4.5 V/nm **(e)** 6.0 V/nm **(f)** 7.5 V/nm

Figure 4.2: Atomistic representation of the final configurations of systems containing water (cyan) and methane (red) in a slit pore of graphene (silver) for different electric fields.

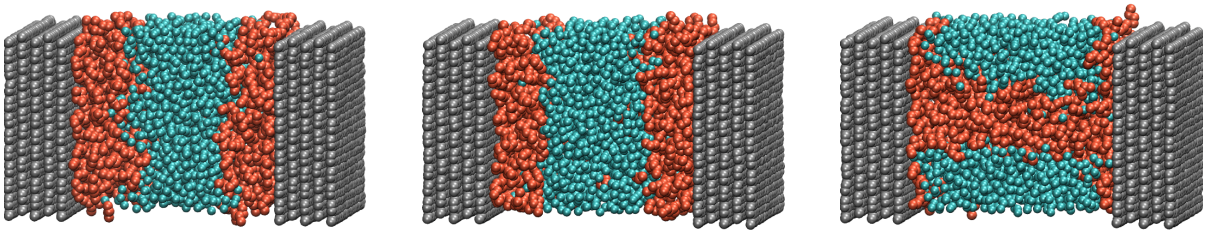

(a) 0.0 V/nm **(b)** 1.5 V/nm **(c)** 3.0 V/nm

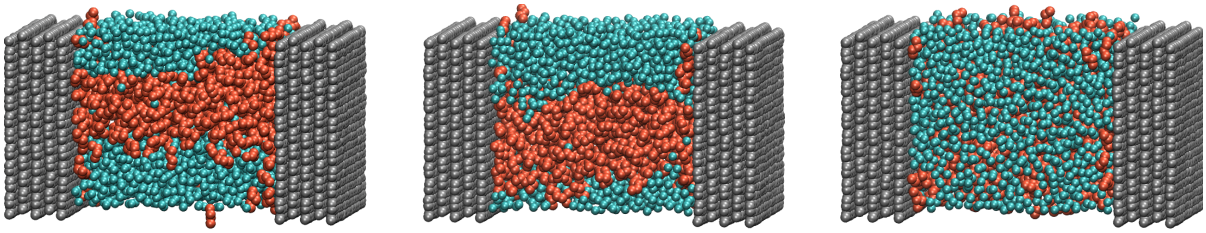

(d) 4.5 V/nm **(e)** 6.0 V/nm **(f)** 7.5 V/nm

Figure 4.3: Atomistic representation of the final configurations of systems containing water (cyan) and *n*-butane (orange) in a slit pore of graphene (silver) for different electric fields.

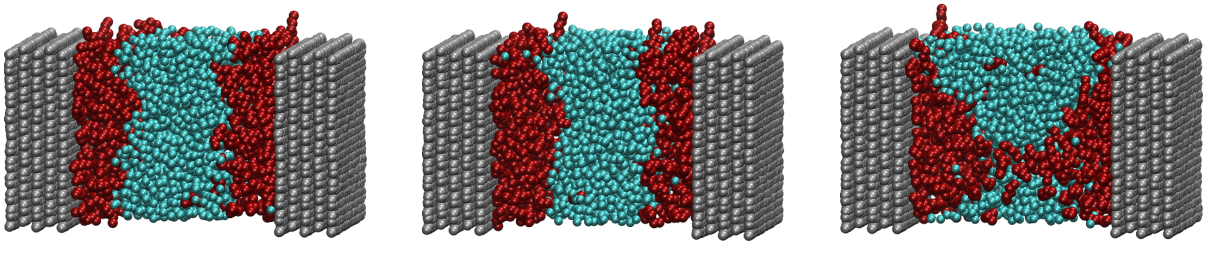

(a) 0.0 V/nm **(b)** 1.5 V/nm **(c)** 3.0 V/nm

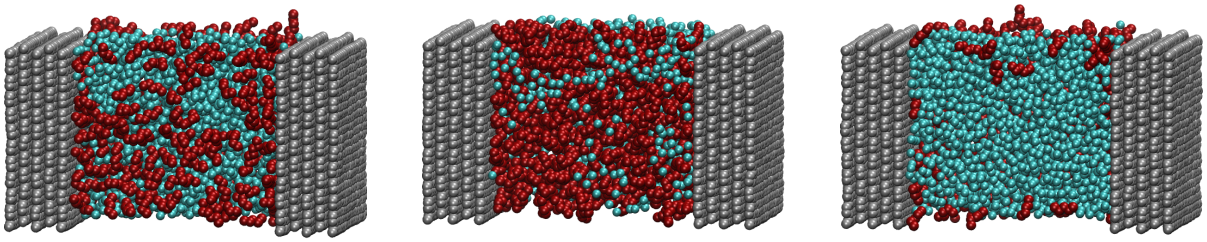

(d) 4.5 V/nm **(e)** 6.0 V/nm **(f)** 7.5 V/nm

Figure 4.4: Atomistic representation of the final configurations of systems containing water (cyan) and *n*-pentane (dark-red) in a slit pore of graphene (silver) for different electric fields.

to analyse the density profile of the systems in all directions, which is shown in the next section.

For comparison, the second approach of the application of the electric field was analysed. In this simulation the field is generated by adding charges to the graphene surface for the mixture water/methane. The result is presented in Figure 4.5.

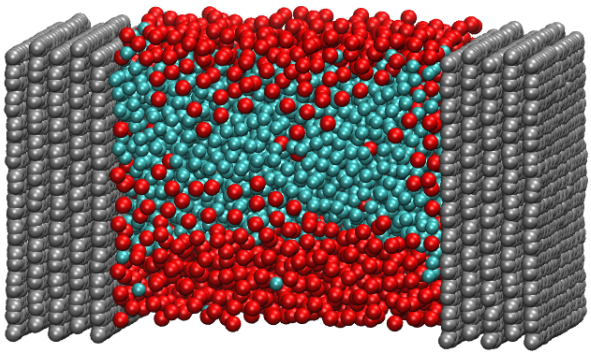

Figure 4.5: Atomistic representation of the final configuration of a system containing water (cyan) and methane (red) in a slit pore of graphene (silver).

From Figure 4.5, the same behavior of the simulations applying the constant potential method is observed. Therefore, the change in the phase separation is also present is this second approach. Therefore, to simplify the simulation preparation, the constant

potential method was adopted for all simulations for further analysis. Results will be presented in the next sections.

4.2 Density Profiles

The density profile showed significant change depending on the electric field applied. The results for the mixture methane/water in the z axis are shown in Figure 4.6 for methane and Figure 4.7 for water.

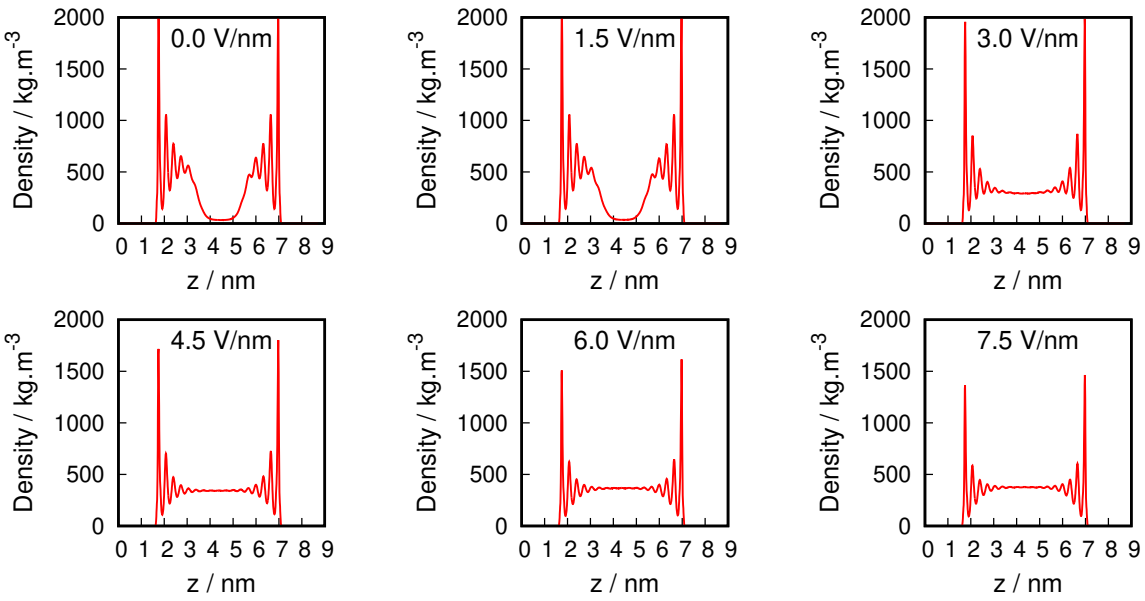

Figure 4.6: Density profiles for methane in mixture methane/water at 573.15 K in the z axis.

The difference in density was not exclusive in the direction of application of the field. For the x direction, the values are presented in Figure 4.8 and for y in Figure 4.9.

The results for the mixture methane/water showed in Figure 4.7 that for electric fields higher than 3 V/nm, water starts adsorbing in graphene while, at the center of the pore, both water and methane can be found. In fact, from Figures 4.8 and 4.9, the phase separation starts occurring in other directions.

For 3 and 4.5 V/nm, the phase separation is in the y axis while for 6 and 7.5 V/nm the separation is in the x axis. The striking result is that applying an external electric field one can essentially change the adsorption profile within the pore, and that is probably an important mechanism for controlling the catalytic process. Graphene is a well-known

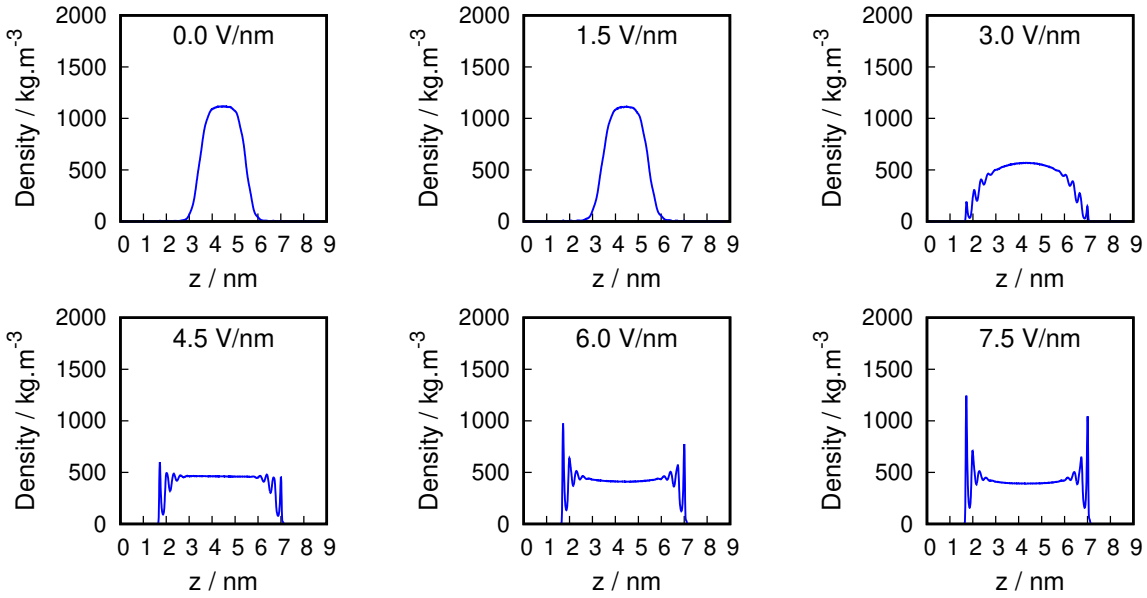

Figure 4.7: Density profiles for water in mixture methane/water at 573.15 K in the z axis.

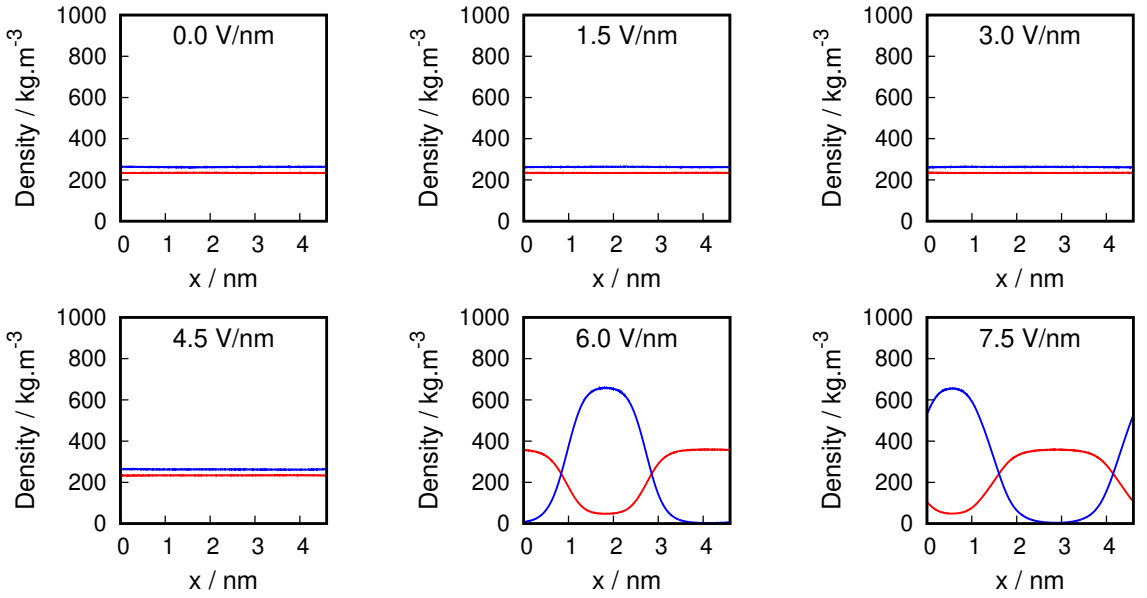

Figure 4.8: Density profiles for mixture methane/water at 573.15 K in the x axis. Red for methane and blue for water.

hydrophobic surface, but at the presence of an external electric field water can be found very close to graphene surface.

The results for the mixture n-butane/water in the z axis are shown in Figure 4.10 for n-butane and Figure 4.11 for water. Regarding axis x and y, the densities are illustrated in Figures 4.12 and 4.13 respectively.

The behavior for n-butane is similar to methane. The difference consists in which axis shows the phase separation in the parallel directions. For 3.0, 4.5, and 6 V/nm, the

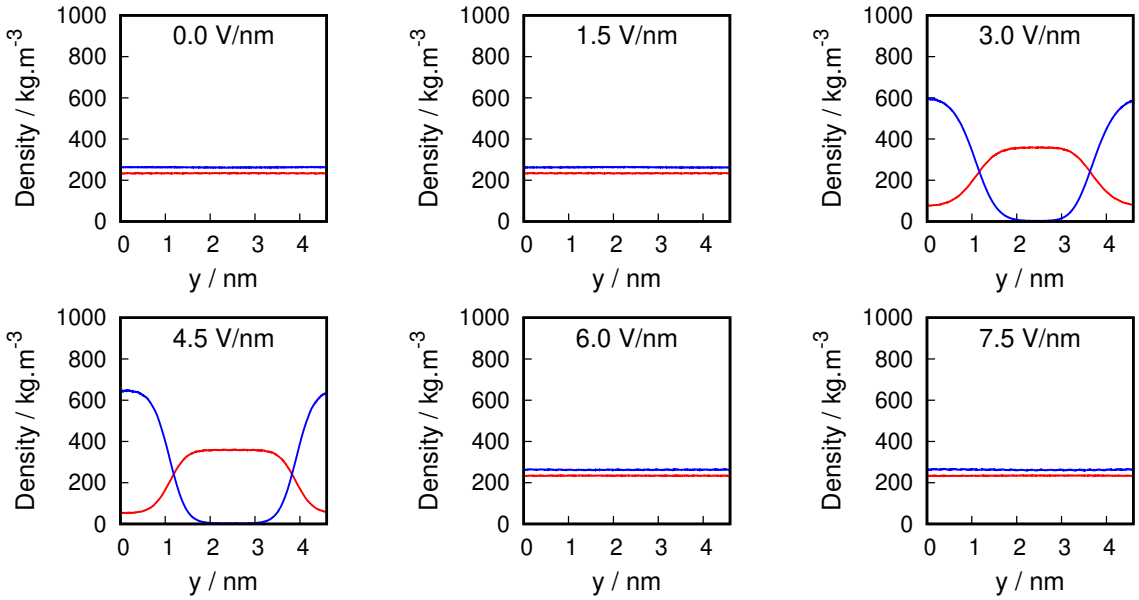

Figure 4.9: Density profiles for mixture methane/water at 573.15 K in the y axis. Red for methane and blue for water.

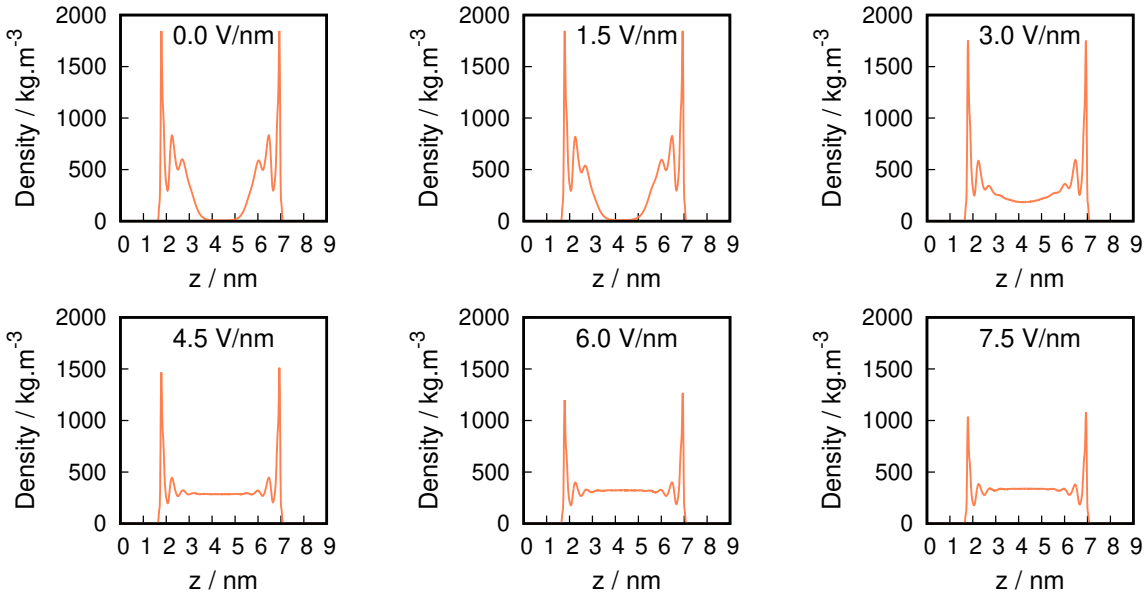

Figure 4.10: Density profiles for n-butane in mixture n-butane/water at 573.15 K in the z axis.

separation is in the y axis while for 7.5 V/nm is in the x axis. But once again the external electric field is able to reorder the adsorption profile within the pore.

The results for the mixture n-pentane/water in the z axis are shown in Figure 4.14 for n-pentane and Figure 4.15 for water. Regarding axis x and y, the densities are shown in Figures 4.16 and 4.17 respectively. The results for n-pentane show that there is also the change in the phase separation for fields higher than 3 V/nm, being almost exclusive to the x direction.

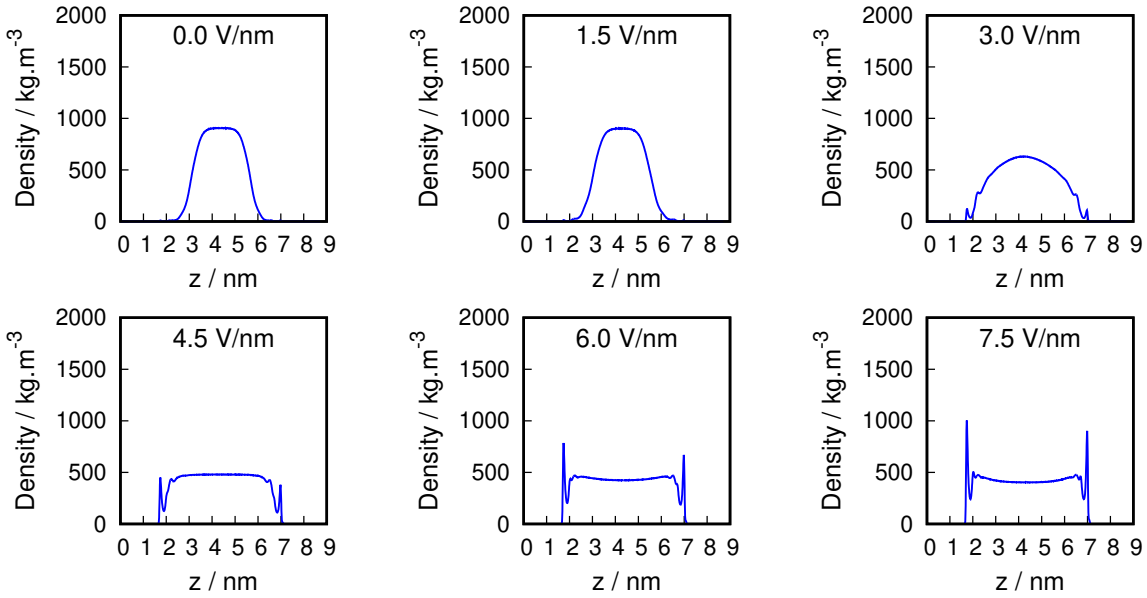

Figure 4.11: Density profiles for water in mixture *n*-butane/water at 573.15 K in the z axis.

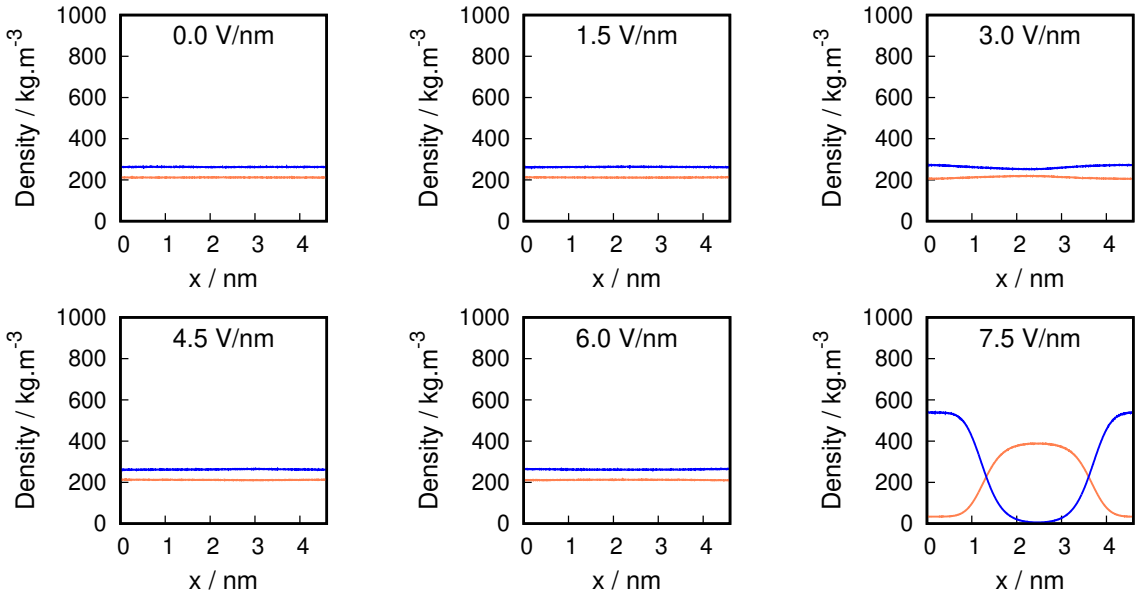

Figure 4.12: Density profiles for mixture *n*-butane/water at 573.15 K in the x axis. Orange for *n*-butane, and blue for water.

One aspect that can be highlighted for the hydrocarbons mixtures is that there is no clear reason to predict which axes occur the phase separation. It can be assumed that the separation between x and y is, in fact, random. The reference axis is z, in which the electric field is applied, but the other two are, for practical effect, indistinguishable.

To analyse this assumption, it is possible to plot a graphic merging the density profiles for each component for the x and y axes when phase separation occurs. For the methane/water mixture, the results can be seen in Figure 4.18, for *n*-butane/water in

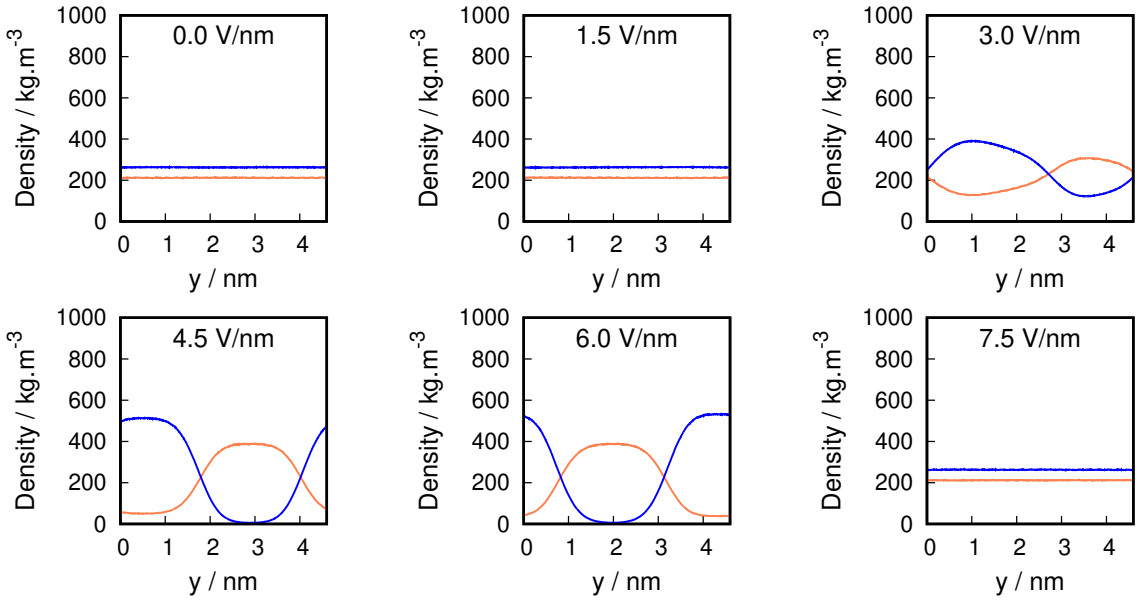

Figure 4.13: Density profiles for mixture *n*-butane/water at 573.15 K in the *y* axis. Orange for *n*-butane, and blue for water.

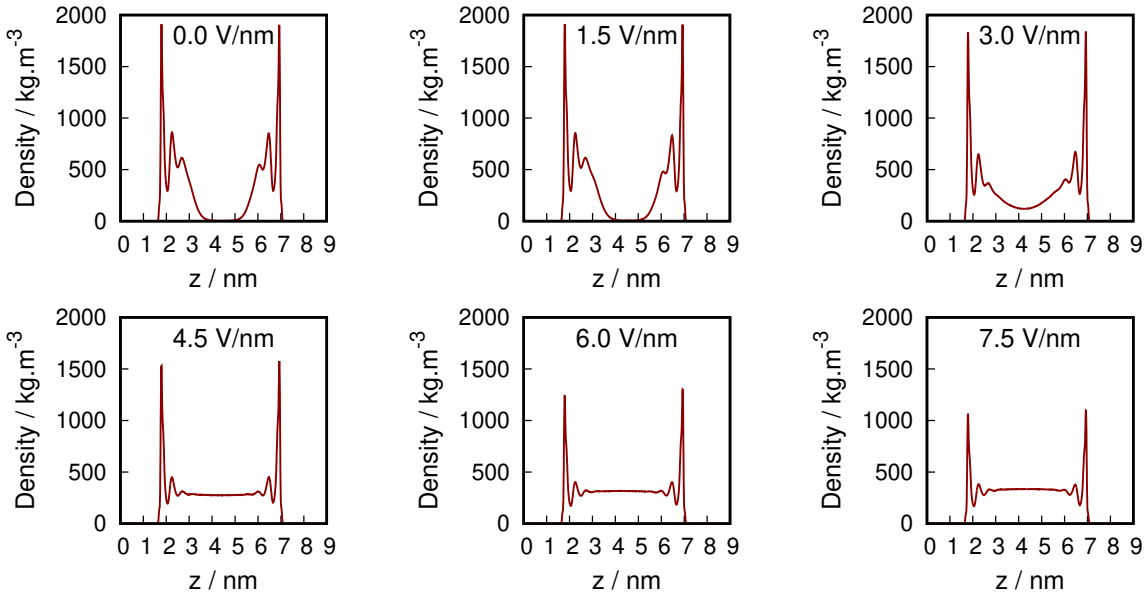

Figure 4.14: Density profiles for *n*-pentane in mixture *n*-pentane/water at 573.15 K in the *z* axis.

Figure 4.19 and for *n*-pentane/water in Figure 4.20.

The results in Figures 4.18, 4.19 and 4.20 show that there is indeed an overlapping of the data for different force-fields. The behavior observed for the curves are similar for the same components regardless of the axis where separation occurs for all three hydrocarbon mixtures.

Although the behavior of the systems have small changes depending on the magnitude of the field applied, it is unclear why the application of a field higher than 3 V/nm

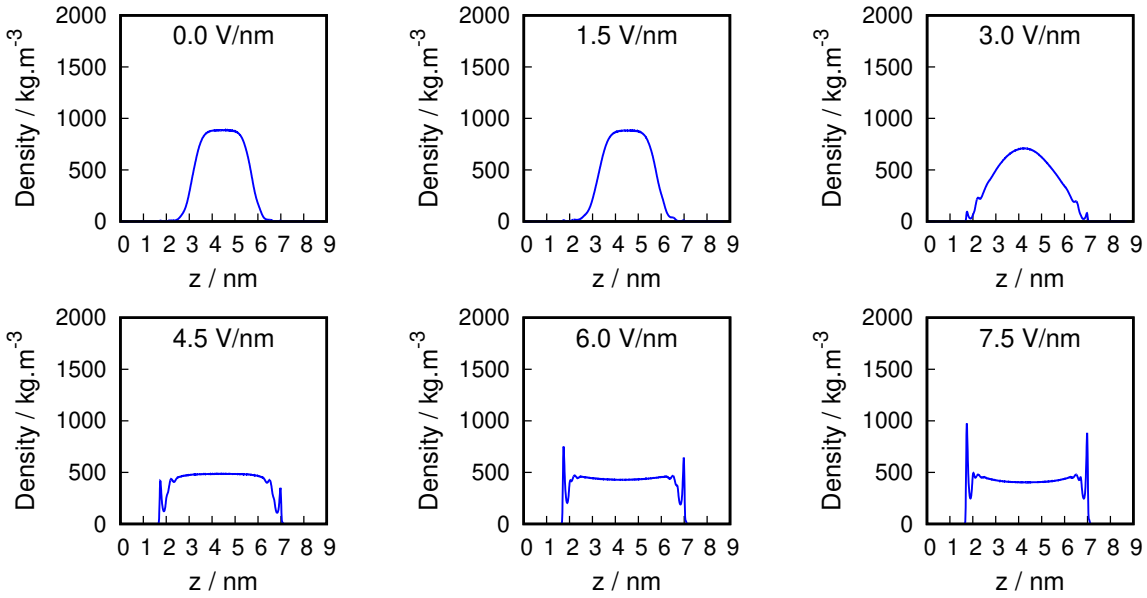

Figure 4.15: Density profiles for water in mixture *n*-pentane/water at 573.15 K in the *z* axis.

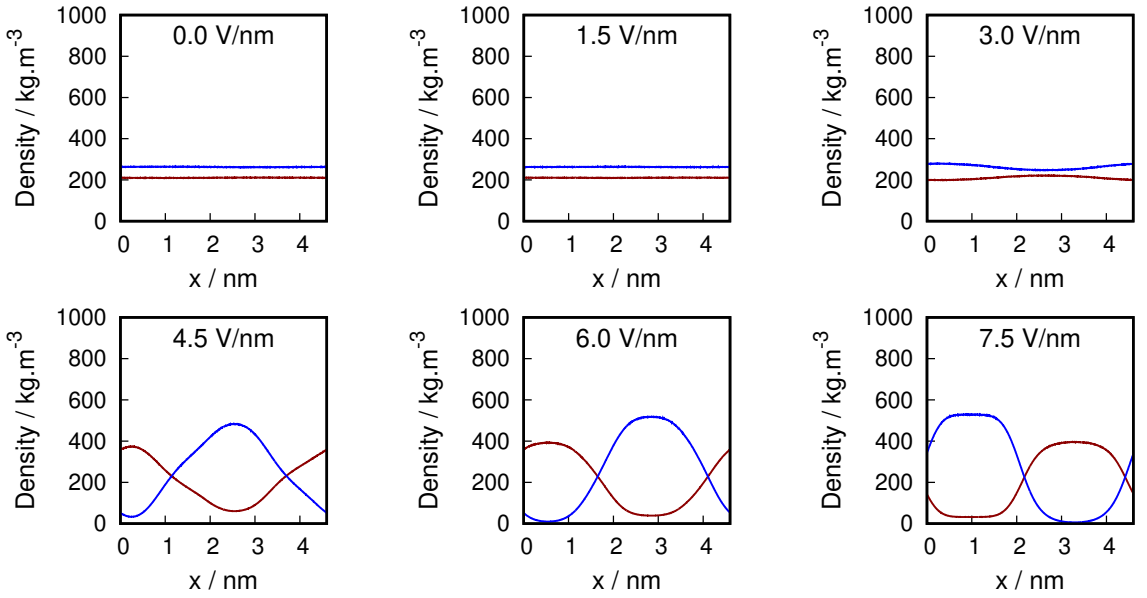

Figure 4.16: Density profiles for mixture *n*-pentane/water at 573.15 K in the *x* axis. Dark-red for *n*-pentane and blue for water.

causes major modifications in phase separation. One aspect that could be related to this changes is the variation of the dipole moment of water.

When considering the rigid TIP4P/2005 model, however, the distance between oxygen and hydrogen are fixed. Therefore, the dipole moment is fixed in 2.305 D [Abascal and Vega, 2005]. The hydrocarbons, as nonpolar molecules, have a dipole moment equal to zero.

Even though the distance between the atoms do not change, orientation of the

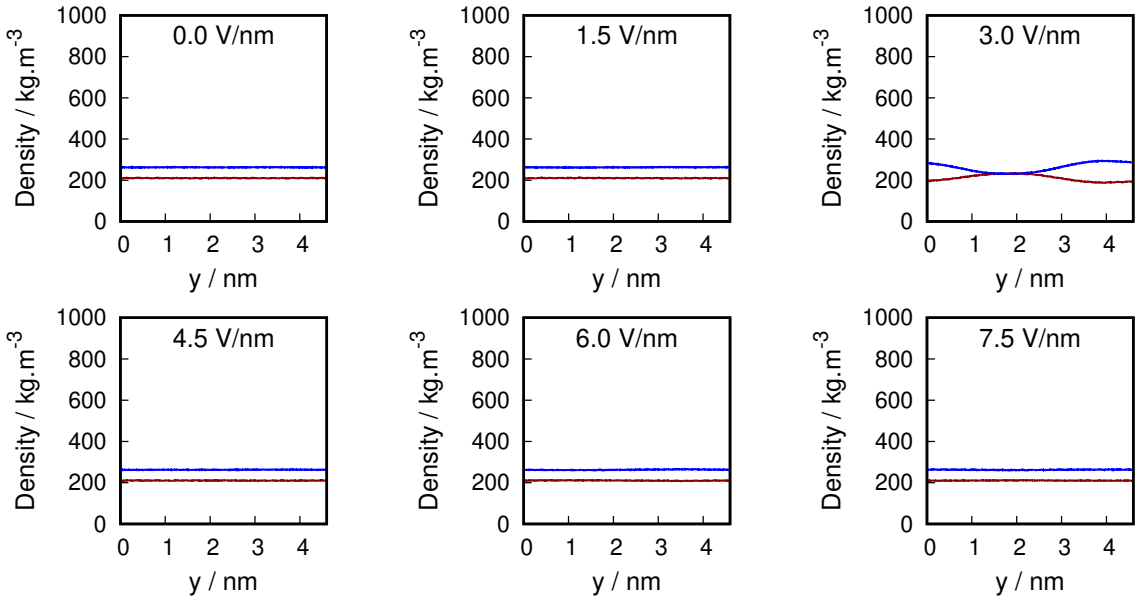

Figure 4.17: Density profiles for mixture *n*-pentane/water at 573.15 K in the *y* axis. Dark-red for *n*-pentane and blue for water.

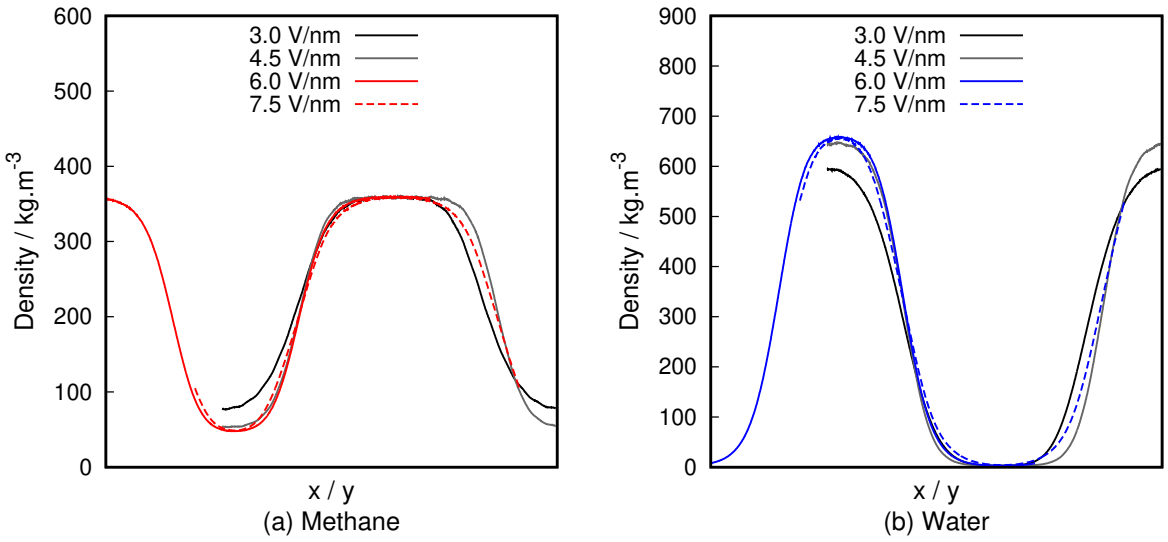

Figure 4.18: Density profiles for mixture methane/water at 573.15 K merging the data for the *x* and *y* axes.

molecules may vary. To analyse this aspect, the order parameter was calculated.

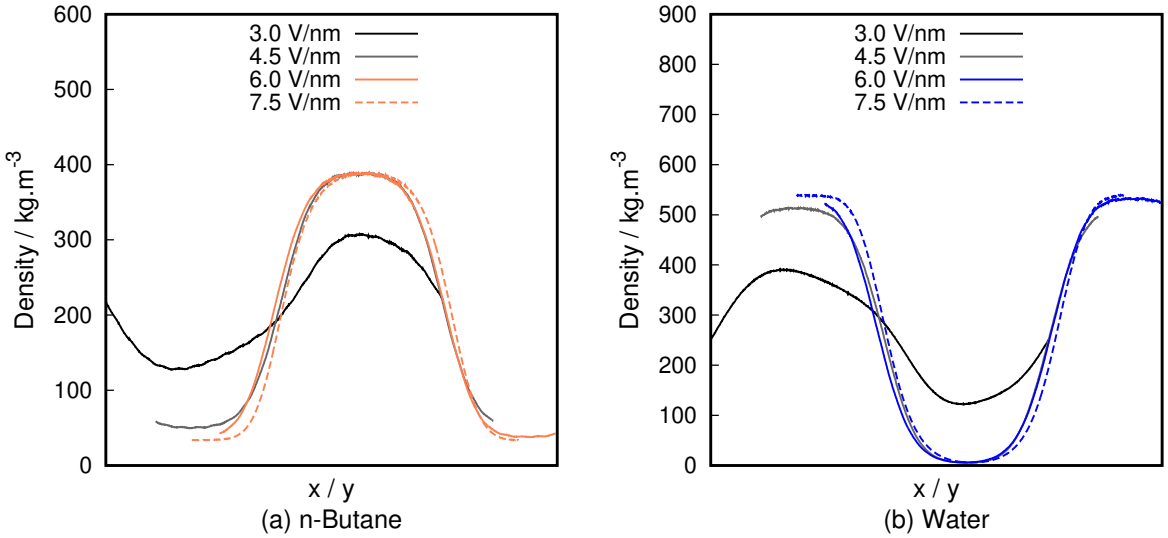

Figure 4.19: Density profiles for mixture *n*-butane/water at 573.15 K merging the data for the x and y axes.

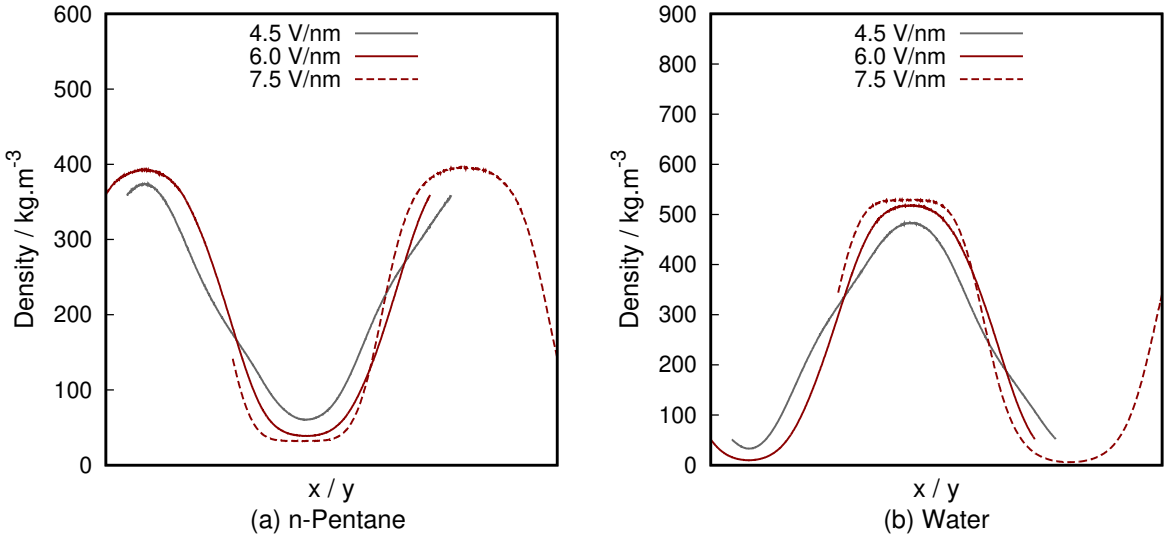

Figure 4.20: Density profiles for mixture *n*-pentane/water at 573.15 K merging the data for the x and y axes.

4.3 Order parameter

The order parameter, S, is a value that can vary from -0.5 to 1 and is related to the orientation of the molecules. If $S = 1$, all molecules are perpendicular to the wall, if S = -0.5 they are parallel to the walls, while if $S = 0$ there is no preferential orientation. The results for the water molecule in methane/water mixture are shown in Figure 4.21.

The results in Figure 4.21 show that the order parameters are close to zero in all

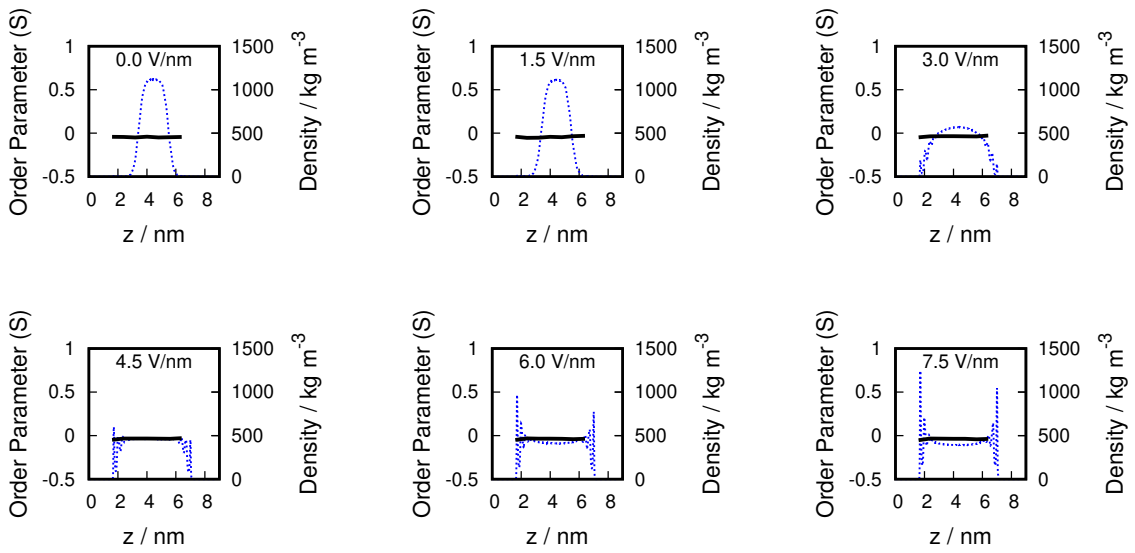

Figure 4.21: Order parameter for water in mixture methane/water at 573.15 K in black. Density profile in blue.

fields. This means the molecules do not have a preferential orientation. Moreover, the increase of the field appear to have no effect in the order parameter distribution.

For *n*-butane/water, the results are presented in Figure 4.22, and for *n*-pentane/water, in Figure 4.23. It is possible to observe the same behavior, as the order parameter is also not changed with the increase of the electric field.

Those results might suggest that the water molecules are not changing the way they interact with graphene. In fact, the molecules are probably not being adsorbed in the wall, but just forced to be placed there by the forces acting upon them.

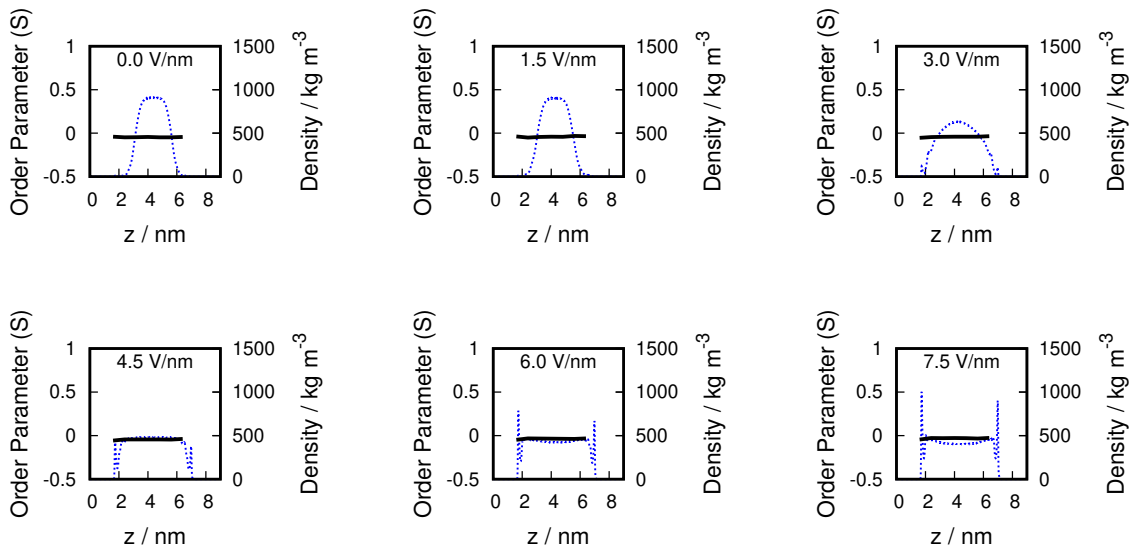

Figure 4.22: Order parameter for water in mixture *n*-butane/water at 573.15 K in black. Density profile in blue.

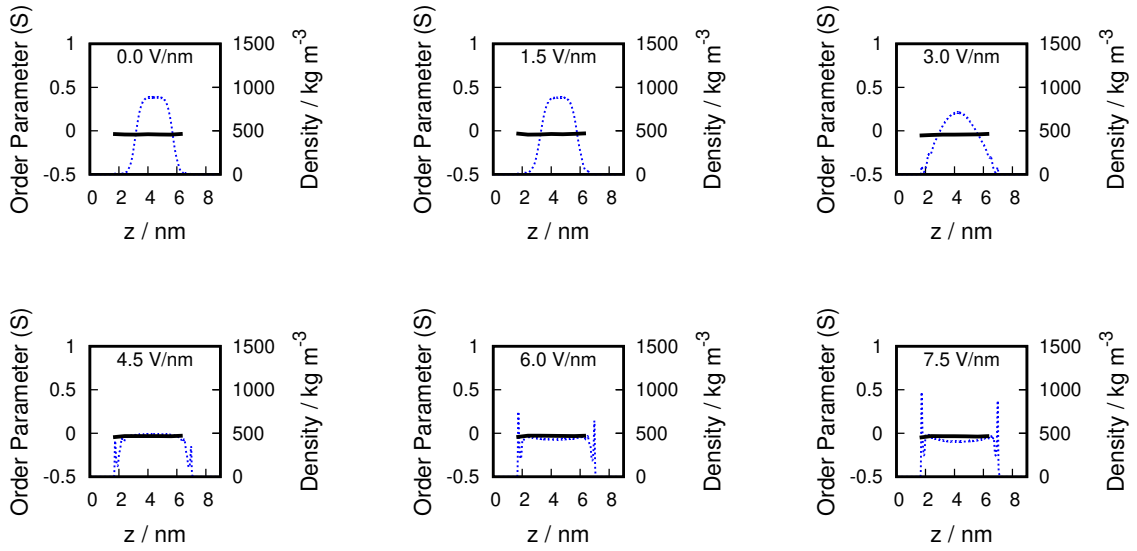

Figure 4.23: Order parameter for water in mixture *n*-pentane/water at 573.15 K in black. Density profile in blue.

4.4 Self-Diffusion

The self-diffusion coefficient is interesting to analyse since it is a transport property and can have great impact in catalysis in general. In electrostatic catalysis this is no different.

In the simulated systems, however, there is the phase separation in an axis different than z, generating an inhomogeneity inside the analysed layer. Therefore, the assumptions

made by Liu et al. [2004] and Franco et al. [2016b] to develop their methodology are not valid in this situation.

To solve this, the Smoluchowski equation should be solved in its analytical form for more than one direction. This solution is not addressed in this study. Another analysis involving the analytical solution of the Smoluchowski equation, however, was done and presented the Appendix A for a different system.

One aspect that can be analysed concerning the diffusion of the system is the survival probability. The survival probability is related to the time the molecules remain in the layers analysed. The faster the molecules diffuse, the faster the survival probability curve reaches zero. In this scenario, it is possible to qualitative analyse if the application of the force field influence the survival probability.

Since the requirements of Equation 2.26 do not include a homogeneous systems, this calculation is still applicable. The results of this study at the center of the pore are presented in Figure 4.24 for methane. Considering that there is the absence of hydrocarbons in the center of the pore for 0 and 1.5 V/nm, no curve is shown for them in these electric fields.

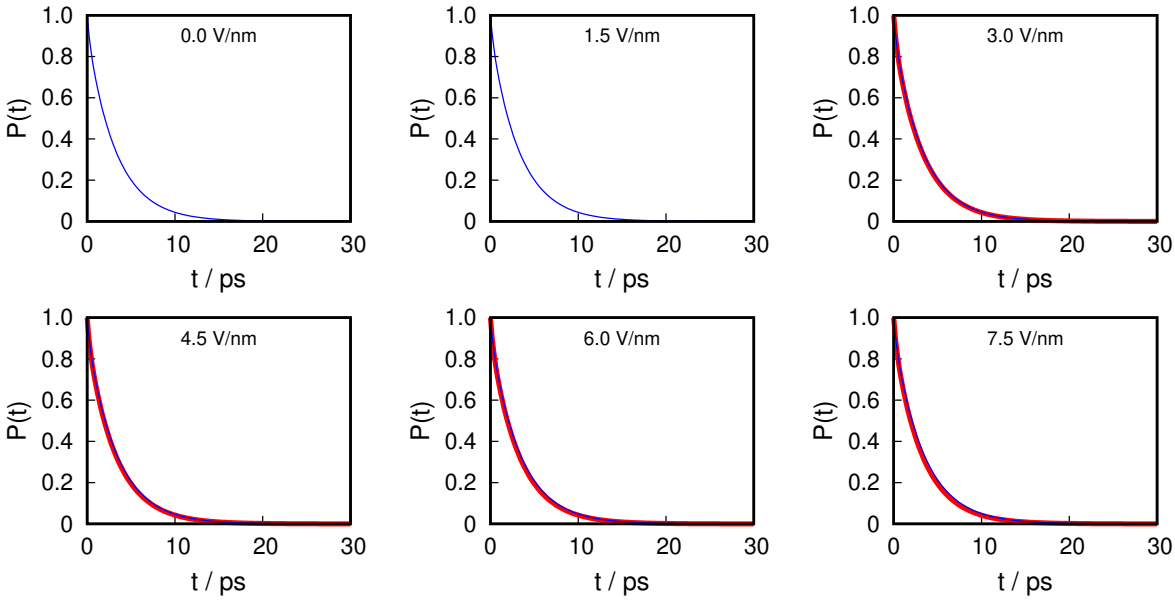

Figure 4.24: Survival probability for mixture methane/water at 573.15 K. Red for methane and blue for water.

In Figure 4.24, the survival probabilities for methane and water show little difference between them. It is also unnoticeable a difference in the curves due to the application of the electric fields.

Expanding this study for *n*-butane and *n*-pentane, however, the results have distinguishable curves between water and the hydrocarbon as can be seen in Figure 4.25 for *n*-butane/water, and in Figure 4.26 for *n*-pentane/water. The difference is directly related to the mass of the molecules. Methane has a molar mass of 16.04 g·mol^{-1} while water 18.02 g·mol^{-1}. The masses of *n*-butane and *n*-pentane are much bigger, 58.12 and 72.15 g·mol^{-1}, respectively.

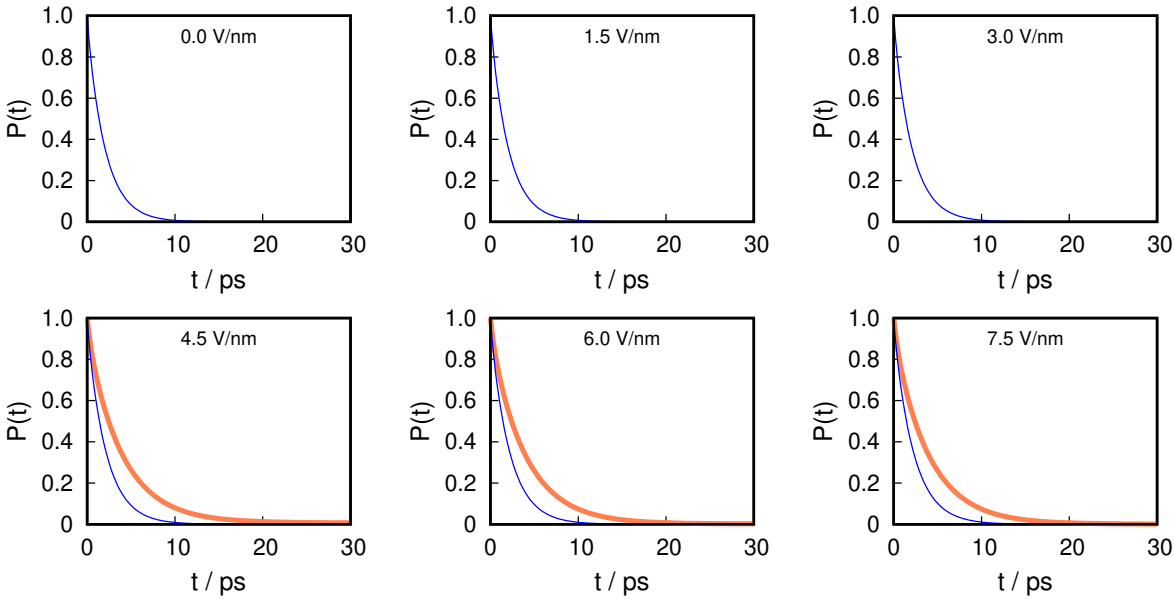

Figure 4.25: Survival probability for mixture *n*-butane/water at 573.15 K. Orange for *n*-butane and blue for water.

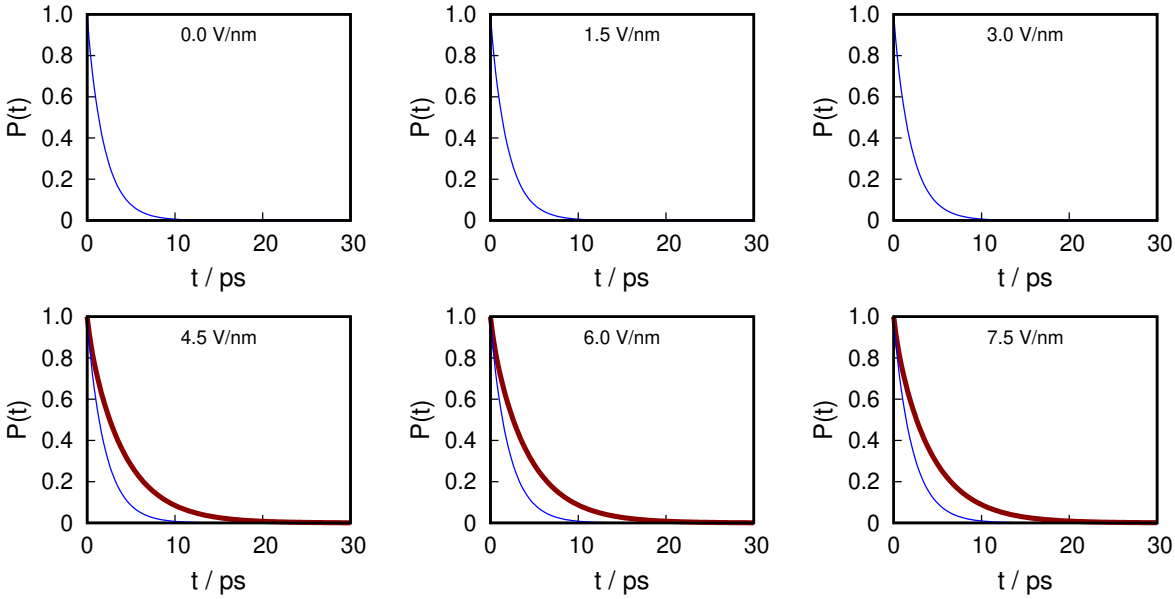

Figure 4.26: Survival probability for mixture *n*-pentane/water at 573.15 K. Dark-red for *n*-pentane and blue for water.

On the other hand, the influence of the field in the survival probability are still not perceptible in Figures 4.25 and 4.26. This result suggests that the field has no significant influence on how fast the molecules diffuse inside the studied layers.

4.5 Further analysis

The explanation to the behavior of the systems as a consequence of the electric field application is still not entirely established.

The considered hypothesis is related to the resultant force caused by the electric field. As already stated, the presence of the electric field adds to the total force of the system a component in the form of Equation 3.7. That means, the force added is proportional to the field and the charge of the particle under that field. For water, the resultant of that force is in the direction of the dipole moment in the axis of the application of the field: z. The representation of the water molecule and the dipole moment can be seen in Figure 4.27.

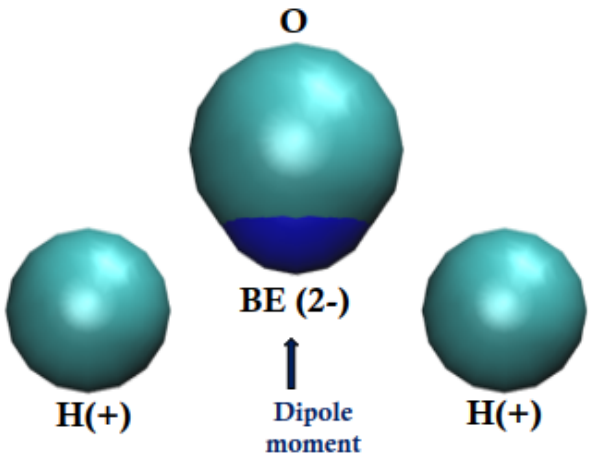

Figure 4.27: Atomistic representation of TIP4P/2005 water model and dipole moment of the molecule.

In Section 4.3 - Order parameter, the order parameter is analysed, and shows that within the layers in z, there is no preferential orientation even when no field is applied. One possibility for the change in the behavior of the molecules is that, for higher fields, the resultant of the electric force generated in z is higher that the repulsive force that cause the phase separation of water and the hydrocarbon or even of water and graphene. Therefore, there is the presence of those molecules in the entire z direction (with water

being found close to the wall) and water grouping according to the orientation of their dipole moment.

In other directions rather than z, the repulsive force between the molecules are still predominant, hence the separation in x or y seen in Section 4.2 - Density Profiles.

5 Final remarks

5.1 Conclusion

Molecular Dynamics simulations were used to analyse the influence of an external electric field in confined media. The systems consisted of the products of the Fischer-Tropsch synthesis focusing on the possibility of applying electrochemical catalysis. The hydrocarbons used were methane, *n*-butane, and *n*-pentane, individually mixed with water, in slit pores of graphene. The considered fields were 1.5, 3.0, 4.5, 6.0 and 7.5 V/nm.

An important change in the configuration of the systems with the application of the field was observed. When no field is applied, there is a phase separation in the perpendicular direction to the graphene surface (z), and hydrocarbons remain close the walls while water remain at the center, since graphene is a hydrophobic surface. With the increase of the field, the phase separation starts to occur in the parallel directions.

Some aspects of the systems were studied to understand this behavior. The study of the order parameter for water showed no change with the field application for the three hydrocarbons, the dipole moment is also unchanged since a rigid water molecule was chosen.

Results for the self-diffusion coefficient were inconclusive since there is an inhomogeneity in the layers in the x and y axis, in disagreement with the assumptions made in the methods chosen for this study. The survival probability, however, was studied and no changed was noted with the change of the external electric field.

Finally, the considered hypothesis is that the additional force caused by the force field overcome the repulsive force between the hydrocarbons or graphene and water in the z direction. In the other directions, the repulsive forces still stand out, causing the phase separation.

5.2 Suggestions for future work

Regarding the FT studies about adsorption and self-diffusion, there is still a lot of ground to cover. Chains of bigger hydrocarbons can be studied, along with their mixtures. Another types of walls can also be analysed such as graphene oxide, which has a lower cost when compared with pure graphene. If extra computational power is available, it is also possible to address these studies applying polarizable force fields for water, for example, to compare the results.

In the systems already studied, there is also the chance to analyse the effect of higher and lower temperatures. Also, the application of oscillating in time electric field is a possibility. Moreover, the study of different pore sizes of graphene can be done.

Additionally, it is also possible to expand the studies of the effect of the electric field to the reaction itself, applying reactive force fields and accounting for the reactants and products. A more advanced step, if results are favorable for the studies mentioned, might be conducting experimental studies.

Apart from FT, the presented results show a perspective to broaden the study for other catalysts that suffer from deposition, for example, and could be removed with the application of an electric field that would change the adsorption preference of the surface.

References

J. L. F. Abascal and C. Vega. A general purpose model for the condensed phases of water: Tip4p/2005. *The Journal of Chemical Physics*, 123(23):234505, 2005. doi: 10.1063/1.2121687.

M. Abraham, B. Hess, D. van der Spoel, and E. Lindahl. Gromacs reference manual, 2018.

B. J. Alder and T. E. Wainwright. Phase transition for a hard sphere system. *The Journal of Chemical Physics*, 27:1208–1209, 1957. doi: 10.1063/1.1743957.

M. P. Allen and D. J. Tildesley. *Computer simulation of liquids*. Oxford university press, 2 edition, 2017.

H. C. Andersen. Molecular dynamics simulations at constant pressure and/or temperature. *The Journal of Chemical Physics*, 72:2384–2393, 1980.

A. C. Aragonès, N. L. Haworth, N. Darwish, S. Ciampi, N. J. Bloomfield, G. G. Wallace, I. Diez-Perez, and M. L. Coote. Electrostatic catalysis of a diels-alder reaction. *Nature*, 531:88–91, 2016. doi: 10.1038/nature16989.

J. L. Aragones, L. G. MacDowell, and C. Vega. Dielectric constant of ices and water: A lesson about water interactions. *The Journal of Physical Chemistry A*, 115(23): 5745–5758, 2011. doi: 10.1021/jp105975c.

G. Bussi, D. Donadio, and M. Parrinello. Canonical sampling through velocity rescaling. *The Journal of Chemical Physics*, 126(1):014101, 2007.

J. Crank. *The mathematics of diffusion*. Oxford University Press, 1975.

T. Darden, D. York, and L. Pedersen. Particle mesh ewald: An $N{\cdot}\log(N)$ method for ewald sums in large systems. *The Journal of Chemical Physics*, 98(12):10089–10092, 1993.

E. M. dos Santos, D. Peyerl, and A. L. A. Netto. *"Opportunities and Challenges of Natural Gas and Liquefied Natural Gas in Brazil"*. Letra Capital, 2021.

M. Elabyouki, D. Bahamon, M. Khaleel, and L. F. Vega. Insights into the transport properties of electrolyte solutions in a hierarchical carbon electrode by molecular dynamics simulations. *The Journal of Physical Chemistry C*, 123(45):27273–27285, 2019. doi: 10.1021/acs.jpcc.9b05620.

J. Fiates, Y. Zhang, L. F. M. Franco, E. J. Maginn, and G. Doubek. Impact of anion shape on li+ solvation and on transport properties for lithium–air batteries: a molecular dynamics study. *Physical Chemistry Chemical Physics*, 22:15842–15852, 2020. doi: 10.1039/D0CP00853B.

M. J. Field. *A Practical Introduction to the Simulation of Molecular Systems*. Cambridge University Press, 2007.

M. Foroutan, S. M. Fatemi, and F. Esmaeilian. A review of the structure and dynamics of nanoconfined water and ionic liquids via molecular dynamics simulation. *European Physical Journal E*, 40(2), 2017. doi: 10.1140/epje/i2017-11507-7.

L. F. M. Franco, M. Castier, and I. G. Economou. Anisotropic parallel self-diffusion coefficients near the calcite surface: A molecular dynamics study. *The Journal of Chemical Physics*, 145:084702, 2016a.

L. F. M. Franco, M. Castier, and I. G. Economou. Diffusion in homogeneous and in inhomogeneous media: A new unified approach. *Journal of Chemical Theory and Computation*, 12(11):5247–5255, 2016b. doi: 10.1021/acs.jctc.6b00653.

D. Frenkel and B. Smit. *Understanding molecular simulation: From algorithms to applications*. Academic Press, 2002.

C. F. Gorin, E. S. Beh, and M. W. Kanan. An electric field–induced change in the selectivity of a metal oxide–catalyzed epoxide rearrangement. *Journal of the American Chemical Society*, 134(1):186–189, 2012. doi: 10.1021/ja210365j.

K. E. Gubbins, Y.-C. Liu, J. D. Moore, and J. C. Palmer. The role of molecular modeling in confined systems: impact and prospects. *Physical Chemistry Chemical Physics*, 13: 58–85, 2011.

Z. Hajjar, M. Doroudian Rad, and S. Soltanali. Novel co/graphene oxide and co/nanoporous graphene catalysts for fischer–tropsch reaction. *Research on Chemical Intermediates*, 43: 1341–1353, 2017. doi: 10.1007/s11164-016-2701-x.

F. Heidari, T. Keshavarzi, and G. Mansoori. Attractive energy contribution to nanoconfined fluids behavior: the normal pressure tensor. *Microfluidics and Nanofluidics*, 10:899–906, 2011. doi: 10.1007/s10404-010-0723-z.

B. Hess, H. Bekker, H. J. C. Berendsen, and J. G. E. M. Fraaije. Lincs: A linear constraint solver for molecular simulations. *Journal of Computational Chemistry*, 18(12):1463–1472, 1997. doi: 10.1002/(SICI)1096-987X(199709)18:12<1463::AID-JCC4>3.0.CO;2-H.

W. G. Hoover. Canonical dynamics: Equilibrium phase-space distributions. *Physical Review A*, 31:1695–1697, 1985. doi: 10.1103/PhysRevA.31.1695.

IEA. Natural gas information: Overview, 2021.

H. Jahangiri, J. Bennett, P. Mahjoubi, K. Wilson, and S. Gua. A review of advanced catalyst development for fischer–tropsch synthesis of hydrocarbons from biomass derived syn-gas. *Catalysis Science and Technology*, 4:2210–2229, 2014. doi: 10.1039/c4cy00327f.

W. L. Jorgensen, J. D. Madura, and C. J. Swenson. Optimized intermolecular potential functions for liquid hydrocarbons. *Journal of the American Chemical Society*, 106(22): 6638–6646, 1984.

W. L. Jorgensen, D. S. Maxwell, and J. Tirado-Rives. Development and testing of the opls all-atom force field on conformational energetics and properties of organic liquids. *Journal of the American Chemical Society*, 118(45):11225–11236, 1996. doi: 10.1021/ja9621760.

S. Karimi, A. Tavasoli, Y. Mortazavi, and A. Karimi. Cobalt supported on graphene – a promising novel fischer–tropsch synthesis catalyst. *Applied Catalysis A: General*, 499: 188–196, 2015. ISSN 0926-860X. doi: 10.1016/j.apcata.2015.04.024.

E. Keshavarzi and M. Kamalvand. Energy effects on the structure and thermodynamic properties of nanoconfined fluids (a density functional theory study). *The Journal of Physical Chemistry B*, 113(16):5493–5499, 2009. doi: 10.1021/jp808466p.

A. Y. Khodakov, W. Chu, and P. Fongarland. Advances in the development of novel cobalt fischer-tropsch catalysts for synthesis of long-chain hydrocarbons and clean fuels. *Chemical Reviews*, 107(5):1692–1744, 2007. doi: 10.1021/cr050972v.

Y.-H. Kim, K. Tang, J. Chang, K. Sharma, S. Yiacoumi, R. Mayes, H. Bilheux, L. Santodonato, and C. Tsouris. Potential limits of capacitive deionization and membrane capacitive deionization for water electrolysis. *Separation Science and Technology*, 54(13):2112–2125, 2019. doi: 10.1080/01496395.2019.1608243.

J. A. Koupaei, S. Hosseini, and F. M. Ghaini. A new optimization algorithm based on chaotic maps and golden section search method. *Engineering Applications of Artificial Intelligence*, 50:201–214, 2016. doi: 10.1016/j.engappai.2016.01.034.

P. Liu, E. Harder, and B. J. Berne. On the calculation of diffusion coefficients in confined fluids and interfaces with an application to the liquid- vapor interface of water. *The Journal of Physical Chemistry B*, 108(21):6595–6602, 2004.

B. F. Machado and P. Serp. Graphene-based materials for catalysis. *Catalysis Science & Technology.*, 2:54–75, 2012. doi: 10.1039/C1CY00361E.

G. A. Mansoori and S. A. Rice. *Confined Fluids: Structure, Properties and Phase Behavior*, chapter 5, pages 197–294. John Wiley and Sons, Ltd, 2014. ISBN 9781118949702. doi: 10.1002/9781118949702.ch5.

M. G. Martin and J. I. Siepmann. Transferable potentials for phase equilibria. 1. United-atom description of n-alkanes. *The Journal of Physical Chemistry B*, 102(14):2569–2577, 1998.

L. Martínez, E. Andrade, R. an Birgin, and J. Martínez. Packmol: A package for building initial configurations for molecular dynamics simulations. *Journal of Computational Chemistry*, 30(13):2157–216, 2009.

R. Meir, H. Chen, W. Lai, and S. Shaik. Oriented electric fields accelerate diels–alder reactions and control the endo/exo selectivity. *ChemPhysChem*, 11(1):301–310, 2010. doi: 10.1002/cphc.200900848.

Z. G. Mills, W. Mao, and A. Alexeev. Mesoscale modeling: solving complex flows in biology and biotechnology. *Trends in Biotechnology*, 31(7):426–434, 2013. doi: 10.1016/j.tibtech.2013.05.001.

J. Mittal, T. M. Truskett, J. R. Errington, and G. Hummer. Layering and position-dependent diffusive dynamics of confined fluids. *Physical Review Letters*, 100(14):145901, 2008.

L. Monticelli and D. P. Tieleman. *Force Fields for Classical Molecular Dynamics*, pages 197–213. Humana Press, Totowa, NJ, 2013.

S. Nosé. A molecular dynamics method for simulations in the canonical ensemble. *Molecular Physics*, 52(2):255–268, 1984. doi: 10.1080/00268978400101201.

J.-H. Oh, J. W. Bae, S.-J. Park, P. K. Khanna, and K.-W. Jun. Slurry-phase fischer–tropsch synthesis using co/al2o3, co/sio2 and co/tio2: Effect of support on catalyst aggregation. *Catalysis Letters*, 130:403–409, 2009. doi: 10.1007/s10562-009-0021-0.

K. D. Papavasileiou, Z. A. Makrodimitri, L. D. Peristeras, J. Chen, G. P. van der Laan, I. Rudra, A. Kalantar, and I. G. Economou. Molecular simulation of n-octacosane–water mixture in titania nanopores at elevated temperature and pressure. *The Journal of Physical Chemistry C*, 120(43):24743–24753, 2016. doi: 10.1021/acs.jpcc.6b07226.

K. D. Papavasileiou, L. D. Peristeras, A. Bick, and I. G. Economou. Molecular dynamics simulation of the n-octacosane–water mixture confined in graphene mesopores: Comparison of atomistic and coarse-grained calculations and the effect of catalyst nanoparticle. *Energy & Fuels*, 35(5):4313–4332, 2021. doi: 10.1021/acs.energyfuels.0c04151.

C. Z. Qiao, S. L. Zhao, H. L. Liu, and W. Dong. Connect the thermodynamics of bulk and confined fluids: Confinement-adsorption scaling. *Langmuir*, 35(10):3840–3847, 2019. doi: 10.1021/acs.langmuir.8b03126.

A. Rahman. Correlations in the motion of atoms in liquid argon. *Physical Review*, 136: A405–A411, 1964. doi: 10.1103/PhysRev.136.A405.

R. Ramanan, D. Danovich, D. Mandal, and S. Shaik. Catalysis of methyl transfer reactions by oriented external electric fields: Are gold–thiolate linkers innocent? *Journal of the American Chemical Society*, 140(12):4354–4362, 2018. doi: 10.1021/jacs.8b00192.

C. Rao, A. Sood, K. Subrahmanyam, and A. Govindaraj. Graphene: The new two-dimensional nanomaterial. *Angewandte Chemie International Edition*, 48(42):7752–7777, 2009. doi: 10.1002/anie.200901678.

T. J. Santos, F. W. Tavares, and C. R. Abreu. Fick diffusion coefficients via molecular dynamics: an alternative approach in the fourier domain. *J. Mol. Liq.*, 329:115460, 2021.

C. Sequeira and D. Santos. Electrochemical routes for industrial synthesis. *Journal of the Brazilian Chemical Society*, 20(3):387–406, 2009. doi: 10.1590/S0103-50532009000300002.

S. Shaik, D. Mandal, and R. Ramanan. Oriented electric fields as future smart reagents in chemistry. *Nature Chemistry*, 8:1091–1098, 2016. doi: 10.1038/nchem.2651.

M. B. Spera and L. F. Franco. The effect of thermal gradients on adsorption. *Fuel*, 295: 120553, 2021. doi: https://doi.org/10.1016/j.fuel.2021.120553.

M. B. Spera, F. N. Braga, R. A. Bartolomeu, I. G. Economou, and L. F. Franco. Diffusion of fluids confined in carbonate minerals: A molecular dynamics simulation study for carbon dioxide and methane–ethane mixture within calcite. *Fuel*, 325:124800, 2022. doi: 10.1016/j.fuel.2022.124800.

Y. W. Tang, K.-Y. Chan, and I. Szalai. Structural and transport properties of an spc/e electrolyte in a nanopore. *The Journal of Physical Chemistry B*, 108:18204–18213, 2004. doi: 10.1021/jp0465985.

J. van de Loosdrecht, F. Botes, I. Ciobica, A. Ferreira, P. Gibson, D. Moodley, A. Saib, J. Visagie, C. Weststrate, and J. Niemantsverdriet. 7.20 - fischer–tropsch synthesis: Catalysts and chemistry. In J. Reedijk and K. Poeppelmeier, editors, *Comprehensive Inorganic Chemistry II (Second Edition)*, pages 525–557. Elsevier, Amsterdam, second edition edition, 2013. ISBN 978-0-08-096529-1. doi: 10.1016/B978-0-08-097774-4.00729-4.

C. Vega and J. L. F. Abascal. Simulating water with rigid non-polarizable models: a general perspective. *Physical Chemistry Chemical Physics*, 13:19663–19688, 2011. doi: 10.1039/C1CP22168J.

T. J. Vlugt, J. P. van der Eerden, M. Dijkstra, B. Smit, and D. Frenkel. *Introduction to Molecular Simulation and Statistical Thermodynamics*. 2008.

J. C. Wang and K. A. Fichthorn. A method for molecular dynamics simulation of confined fluids. *Journal of Chemical Physics*, 112(19):8252–8259, 2000. doi: 10.1063/1.481430.

A. Warshel, P. K. Sharma, M. Kato, Y. Xiang, H. Liu, and M. H. Olsson. Electrostatic basis for enzyme catalysis. *Chemical Reviews*, 106(8):3210–3235, 2006. doi: 10.1021/cr0503106.

S. Wei, C. Zhong, and H. Su-Yi. Molecular dynamics simulation of liquid water under the influence of an external electric field. *Molecular Simulation*, 31:555–559, 2005. doi: 10.1080/0892702500138483.

D. A. Wood, C. Nwaoha, and B. F. Towler. Gas-to-liquids (gtl): A review of an industry offering several routes for monetizing natural gas. *Journal of Natural Gas Science and Engineering*, 9:196–208, 2012. ISSN 1875-5100. doi: 10.1016/j.jngse.2012.07.001.

S. Xiao, S. A. Edwards, and F. Gräter. A new transferable forcefield for simulating the mechanics of CaCO3 crystals. *The Journal of Physical Chemistry C*, 115(41): 20067–20075, 2011.

W. Xiong, Y. L. Zhao, J. H. Qin, S. L. Huang, and L. H. Zhang. Phase equilibrium modeling for confined fluids in nanopores using an association equation of state. *Journal of Supercritical Fluids*, 169:105118, 2021. doi: 10.1016/j.supflu.2020.105118.

Y.-X. Yu, F.-Q. You, Y. Tang, G.-H. Gao, and Y.-G. Li. Structure and adsorption of a hard-core multi-yukawa fluid confined in a slitlike pore:grand canonical monte carlo simulation and density functional study. *The Journal of Physical Chemistry B*, 110(1): 334–341, 2006. doi: 10.1021/jp055299s.

Appendix

APPENDIX A – Additional Studies

These additional studies aimed an exploratory understanding of the methodology developed by Franco et al. [2016b] for the calculation of the perpendicular component of the self-diffusion coefficient. The systems simulated were different from the ones used in the main topics, due to the contribution for the article of Spera et al. [2022] and for that is addressed as an Appendix. In this study, pure methane and ethane confined between two parallel plates of calcite were analysed.

A.1 Simulation details

The system consists of methane and ethane confined in a slit pore of calcite, $CaCO_3$, as a representation of a shale gas reservoir. The considered calcite plane xyz dimensions were 4.990 nm x 4.856 nm x 1.212 nm with fixed pore size in the z axis of $H = 3.5$ nm.

Simulations were carried out for comparison for pure methane and pure ethane. The overall density of all the systems was set as 250 kg·m^{-3}. The code used to perform the computer simulations was GROMACS 2018.1.

Initially, the simulation of bulk fluids was performed as a validation. The equilibrated configuration of those systems was used as the first input for the fluids to be confined between the walls. Prior to the MD simulation, the steepest descent method was used with a maximum number of iterations equal to 5000 to relax the initial configuration. Then, an equilibration step was performed in the canonical ensemble for 20 ns, followed by 50 ns of production steps in the same ensemble.

The numerical integration was done using the Leap-Frog algorithm with a time step of 2 fs. Positions and velocities were stored every 0.2 ps. Velocity-rescale thermostat was used to keep the temperature of the entire system at 375 K with relaxation time of $\tau_T = 1.0$ ps.

The force fields applied were TraPPE-UA for the hydrocarbons [Martin and Siepmann, 1998] and Xiao et al. [2011] for the calcite crystal, with a cutoff radius of 1.0 nm.

The TraPPE-UA force field describes single interaction sites, called pseudo-atoms,

representing an atom of carbon surrounded by all its bonded hydrogens [Martin and Siepmann, 1998]. The pseudo-atoms used in this system were CH_4, CH_3, and CH_2. The force field for calcite, however, treats every atom (Ca, C and O) individually [Xiao et al., 2011]. In both cases, the Lennard-Jones potential function is applied. The parameters taken from these studies are reported in Table A.1.

Table A.1: Lennard-Jones parameters.

Particle	C_6 (kJ· mol^{-1}· nm^{-6})	C_{12} (kJ· mol^{-1}· nm^{-12})	Charge (e)
CH_4	1.33×10^{-2}	3.57×10^{-5}	0
CH_3	9.06×10^{-3}	2.52×10^{-5}	0
CH_2	5.81×10^{-3}	2.21×10^{-5}	0
Ca	1.42×10^{-3}	2.52×10^{-7}	+1.668
C	4.61×10^{-3}	1.44×10^{-5}	+0.999
O	2.03×10^{-3}	1.77×10^{-6}	−0.889

The LJ parameters for the interaction between the fluid and the wall were calculated applying geometrical combining rules as shown in Equations 3.1 and 3.2.

Concerning the C_6 and C_{12} crossed parameters, they were calculated by Equations A.1 and A.2. The values of the crossed parameters are reported in Table A.2.

$$C_{6ij} = \left(C_{6i}C_{6j}\right)^{1/2}, \tag{A.1}$$

$$C_{12ij} = \left(C_{12i}C_{12j}\right)^{1/2}. \tag{A.2}$$

Regarding bonded interactions, for both force fields, the bonded potentials include bonds, angles, and torsions. For hydrocarbons, bond lengths between pseudo-atoms were fixed as 1.54 Å, and C−O bonds from the carbonate molecule are fixed as 1.18 Å. To keep the bonds fixed, LINCS constraint algorithm [Hess et al., 1997] was applied.

Bond angles were characterized as harmonic potentials, and the potential function is expressed in Equation A.3, where θ_{ijk} is the angle between 3 atoms i, j, and k.

$$u_{\text{angles}} = \sum_{\text{angles}} \frac{1}{2} k_\theta (\theta_{ijk} - \theta_{\text{eq}})^2. \tag{A.3}$$

The force constant, k_θ, is equal to 519.625 kJ·mol^{-1}·rad^{-2} for hydrocarbons and 1852 kJ·mol^{-1}·rad^{-2} for carbonate. On the other hand, the equilibrium angle, θ_{eq}, determined for hydrocarbons is 114° and for O−C−O is 120°.

Table A.2: Crossed Lennard-Jones parameters.

Particle i	**Particle j**	C_6 (kJ· mol^{-1}· nm^{-6})	C_{12} (kJ· mol^{-1}· nm^{-12})
CH_4	CH_4	1.33×10^{-2}	3.57×10^{-5}
CH_3	CH_3	9.06×10^{-3}	2.52×10^{-5}
CH_2	CH_2	5.81×10^{-3}	2.21×10^{-5}
CH_4	CH_3	1.10×10^{-2}	3.00×10^{-5}
CH_4	CH_2	8.80×10^{-3}	2.82×10^{-5}
CH_3	CH_2	7.27×10^{-3}	2.37×10^{-5}
Ca	Ca	1.42×10^{-3}	2.52×10^{-7}
Ca	O	0	9.49×10^{-7}
C	C	1.43×10^{-2}	4.61×10^{-6}
C	O	3.08×10^{-4}	9.04×10^{-10}
O	O	5.21×10^{-5}	5.94×10^{-7}

The torsion potential is a function of dihedral angles, ϕ, and is described for hydrocarbons [Martin and Siepmann, 1998] by Equation A.4:

$$u_{\text{torsions}} = c_1[1 + \cos\phi] + c_2[1 - \cos(2\phi)] + c3[1 + \cos(3\phi)], \tag{A.4}$$

with $c_1/k_B = 335.03$ K, $c_2/k_B = -68.19$ K, and $c_3/k_B = 791.32$ K.

For the carbonate ion, Equation A.5 describes the torsion potential [Xiao et al., 2011], with $k_\phi = 28.9$ kJ·mol^{-1}.

$$u_{\text{torsions}} = \sum_{\text{torsions}} \frac{1}{2} k_\phi (1 - \cos(2\phi)). \tag{A.5}$$

The nonbonded interactions were computed based on a neighbor list; a list of non-bonded particles in a certain radius. Neighbor searching was performed with the Verlet cut-off scheme up to the distance of 1 nm. The grid research type was used, and Periodic Boundary Conditions were applied in all directions.

To compute electrostatic Coulombic interactions, Particle Mesh Ewald method [Darden et al., 1993] was used with a Fourier spacing of 0.16 nm in the confined systems. The distance applied for the cut-off was 1 nm. For homogeneous systems, the Coulomb type used was cut-off and tail corrections for energy and pressure were applied.

A.2 Tolerance time

Revisiting section 2.6- Diffusion of chapter 2- Theoretical background, the first aim was to evaluate the influence of a tolerance time in the calculation of the survival probability to obtain the self-diffusion coefficient. The survival probability is calculated considering multiple time origins as a dependence of how many molecules remain in the original layer Ω after each time step, as shown by Equation 2.26.

The addition of a tolerance time is done by considering the possibility that the molecule return to the layer after a short period of time, implying that the displacement was reasonably small. The periods of time of tolerance (dt) calculated were from zero to four time steps, where zero is the original study. The results for the self-diffusion coefficients are shown for comparison in Table A.3 for methane and in Table A.4 for ethane.

Table A.3: Values of the self-diffusion coefficient as a function of the tolerance time for methane in a 3.5 nm pore of calcite.

dt	D_{Wall} / $\text{m}^2\cdot\text{s}^{-1}$			D_{Center} / $\text{m}^2\cdot\text{s}^{-1}$		
	$D_{xx} \times 10^8$	$D_{yy} \times 10^8$	$D_{zz} \times 10^9$	$D_{xx} \times 10^8$	$D_{yy} \times 10^8$	$D_{zz} \times 10^8$
0	1.85	2.06	7.64	7.40	7.64	1.58
1	1.84	2.11	0.423	7.35	7.45	1.38
2	1.84	2.15	0.413	7.62	7.59	1.22
3	1.88	2.15	0.407	7.58	7.81	1.10
4	1.90	2.17	0.409	7.70	7.89	1.03

Table A.4: Values of the self-diffusion coefficient as a function of the tolerance time for ethane in a 3.5 nm pore of calcite.

dt	D_{Wall} / $\text{m}^2\cdot\text{s}^{-1}$			D_{Center} / $\text{m}^2\cdot\text{s}^{-1}$		
	$D_{xx} \times 10^8$	$D_{yy} \times 10^8$	$D_{zz} \times 10^9$	$D_{xx} \times 10^8$	$D_{yy} \times 10^8$	$D_{zz} \times 10^8$
0	1.33	1.84	2.85	6.44	6.08	1.18
1	1.35	1.85	0.058	6.32	6.05	1.08
2	1.36	1.86	0.058	6.14	6.26	0.981
3	1.37	1.87	0.057	6.12	6.15	0.904
4	1.38	1.87	0.057	6.20	6.15	0.843

From Tables A.3 and A.4, the values of the self-diffusion coefficient that are most

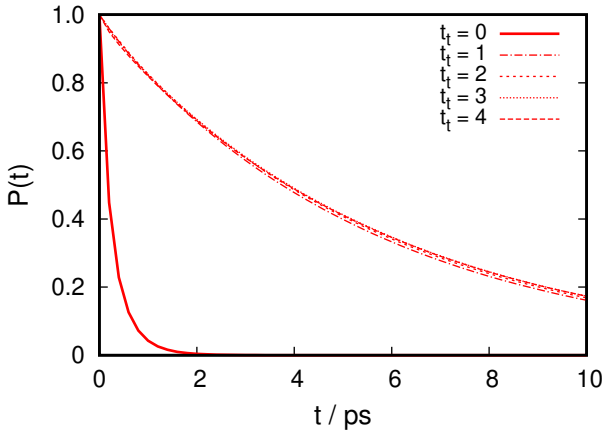

Figure A.1: Survival probability behavior close to the wall for methane, within a 3.5 nm pore of calcite, in the perpendicular direction.

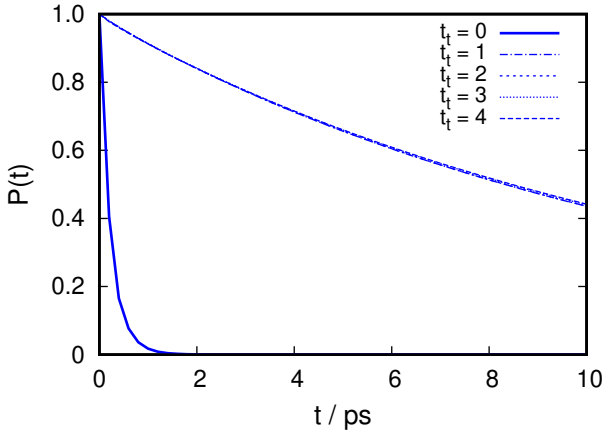

Figure A.2: Survival probability behavior close to the wall for ethane, within a 3.5 nm pore of calcite, in the perpendicular direction.

influenced by the addition of the tolerance time are the ones in the perpendicular direction. While parallel coefficients differ from the original one only up to 5 %, the perpendicular coefficient in the center reaches 35 % and the one close to the wall 95 % of difference.

The source of this difference can be seen in Figure A.1 for methane and Figure A.2 for ethane. The addition of the tolerance time increases the time needed for the survival probability to reach zero, as molecules remain for longer periods of time in the layer. This result is probably more marked because there are less molecules in the layer considered for the perpendicular coefficient calculation than the parallels ones, due to the condition of linear density profile.

This difference can be also observed analysing α and the residence time (τ_r) in Tables A.5 and A.6. Although α remains the same, there are major differences between the residence times closer to the wall, as this value is the integral in time of the survival

probability (Equation 2.30). That result may suggest that the method proposed by Franco et al. [2016b] may not be applicable to the addition of the tolerance time, mostly because of the assumption of a linear potential of mean force.

Table A.5: Values of α and the residence time (τ_r) for methane.

t_t	Wall		Center	
	α	τ_r / ps	α	τ_r / ps
0	5.13	0.30	12.00	1.31
1	5.13	5.38	12.00	1.50
2	5.13	5.50	12.00	1.71
3	5.13	5.58	12.00	1.88
4	5.13	5.56	12.00	2.03

Table A.6: Values of α and the residence time (τ_r) for ethane.

t_t	Wall		Center	
	α	τ_r / ps	α	τ_r / ps
0	11.14	0.24	12.00	1.76
1	11.14	12.02	12.00	1.93
2	11.14	12.04	12.00	2.12
3	11.14	12.16	12.00	2.30
4	11.14	12.21	12.00	2.47

In this scenario, a deeper look into method proposed by Franco et al. [2016b] is needed, more specifically back to the Smoluchowski equation.

A.3 Smoluchowski Equation

The Smoluchowski equation (Equation 2.22), as already established, is a more appropriate description of the particle distribution in confined systems. The methodology proposed by Franco et al. [2016b] was developed by solving analytically the Smoluchowski equation for a linear potential of mean force and for that, the α parameter was deduced. The specific influence of the addition of the tolerance time on that parameter, however, is difficult to account for in the deduction of the equations.

Therefore, it is proposed to apply the discretization of the Smoluchowski Equation to analyse how the tolerance time affects the diffusion coefficient and if corrections in α

would be needed. The discretized equation (A.6) is also presented by Franco et al. [2016b] applying the forward in time and centered in space (FTCS) method.

$$p_{i+1,j} = p_{i,j} + \frac{D\partial t}{(\partial r)^2}[\phi_{0,j}p_{i,j+1} + \phi_{1,j}p_{i,j} + \phi_{2,j}p_{i,j-1}], \tag{A.6}$$

where i is the index for time evolution, j is the index for spatial discretization, ∂t is the increment in time, ∂r is the increment in space, D is the self-diffusion coefficient, $p_{i,j}$ is the probability distribution function at position j and at time i. Moreover, there are the following definitions:

$$\phi_{0,j} = 1 - \frac{1}{4}\ln\left(\frac{\rho_{j+1}}{\rho_{j-1}}\right), \tag{A.7}$$

$$\phi_{1,j} = -\left[2 - \frac{\partial r}{2}\ln\left(\frac{\rho_{j+1}\rho_{j-1}}{(\rho_j)^2}\right)\right], \tag{A.8}$$

$$\phi_{2,j} = 1 + \frac{1}{4}\ln\left(\frac{\rho_{j+1}}{\rho_{j-1}}\right), \tag{A.9}$$

where ρ_j is the discretized density obtained from Molecular Dynamics simulations.

The survival probability can be obtained by the integral in space of Equation A.6. In this case, the survival probability is an implicit function of D. To compute D, the curve obtained by the integration of Equation A.6 is compared to the one obtained by Equation 2.26 as a function of time and the coefficient is adjusted to minimize the mean square deviation, using the golden search algorithm [Koupaei et al., 2016]. The studies were made only in the perpendicular direction, for the case closer to the wall.

The result of the Smoluchowski discretization in comparison to the method derived by Franco et al. [2016b] is shown in Figures A.3 and A.4.

Considering that the self-diffusion coefficient obtained from the Smoluchowski discretization is not a function of the hypotheses assumed by Franco et al. [2016b], this value will be considered as reference: $D = 1.50 \times 10^{-10}$ m^2·s^{-1}. In this scenario, Equation 2.28 may be rewritten as Equation A.10:

$$\alpha = \frac{L^2}{D_\perp \tau_r}. \tag{A.10}$$

The new values of α are show in Table A.7.

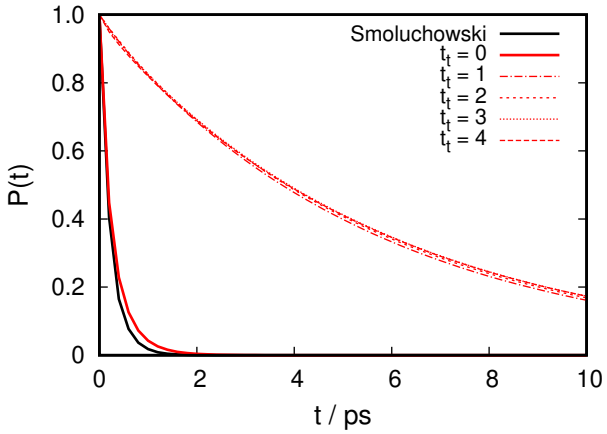

Figure A.3: Survival probability behavior close to the wall for methane, in the perpendicular direction. Red for Franco et al. [2016b] method and black for Smoluchowski discretization

.

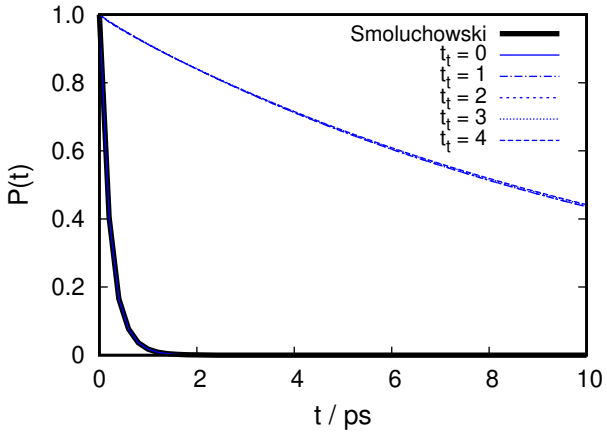

Figure A.4: Survival probability behavior close to the wall for ethane, in the perpendicular direction. Blue for Franco et al. [2016b] method and black for Smoluchowski discretization

.

Table A.7: Values of α after Smoluchowski correction.

t_t	**methane** α	**ethane** α
1	14.46	4.27
2	14.13	4.27
3	13.94	4.22
4	13.99	4.20

A.4 Final remarks

In conclusion, this is still a work in progress. It was clear that the survival probability behavior drastically change with the addition of the tolerance time. The reason for that

behavior, however, is not completely clear. The hypothesis raised that the α value should be corrected is one possible explanation. It is still unclear how these results may or may not affect the application of the methodology developed by Franco et al. [2016b]. A deeper look into this methodology is needed, but is not in the scope of this dissertation.